Exciton-polaritons in cuprous oxide: Theory and comparison with experiment

Frank Schweiner, Jan Ertl, Jörg Main, and Günter Wunner
Institut für Theoretische Physik 1, Universität Stuttgart, 70550 Stuttgart, Germany

Christoph Uihlein
Experimentelle Physik 2, Technische Universität Dortmund, 44221 Dortmund, Germany
(Received 15 August 2017; revised manuscript received 17 October 2017; published 4 December 2017)

The observation of giant Rydberg excitons in cuprous oxide (Cu_2O) up to a principal quantum number of $n = 25$ by T. Kazimierczuk *et al.* [Nature (London) **514**, 343 (2014)] inevitably raises the question whether these quasiparticles must be described within a multipolariton framework since excitons and photons are always coupled in the solid. In this paper we present the theory of exciton-polaritons in Cu_2O. To this end we extend the Hamiltonian which includes the complete valence-band structure, the exchange interaction, and the central-cell corrections effects, and which has been recently deduced by F. Schweiner *et al.* [Phys. Rev. B **95**, 195201 (2017)], for finite values of the exciton momentum $\hbar K$. We derive formulas to calculate not only dipole but also quadrupole oscillator strengths when using the complete basis of F. Schweiner *et al.*, which has recently been proven as a powerful tool to calculate exciton spectra. Very complex polariton spectra for the three orientations of $\boldsymbol{K}$ along the axes [001], [110], and [111] of high symmetry are obtained and a strong mixing of exciton states is reported. The main focus is on the $1S$ ortho-exciton-polariton, for which pronounced polariton effects have been measured in experiments. We set up a 5×5 matrix model, which accounts for both the polariton effect and the K-dependent splitting, and which allows treating the anisotropic polariton dispersion for any direction of $\boldsymbol{K}$. We especially discuss the dispersions for $\boldsymbol{K}$ being oriented in the planes perpendicular to $[1\bar{1}0]$ and [111], for which experimental transmission spectra have been measured. Furthermore, we compare our results with experimental values of the K-dependent splitting, the group velocity, and the oscillator strengths of this exciton-polariton. The results are in good agreement. This proves the validity of the 5×5 matrix model as a useful theoretical model for further investigations on the $1S$ ortho-exciton-polariton.

DOI: 10.1103/PhysRevB.96.245202

I. INTRODUCTION

Excitons are Coulomb-bound pairs of a positively charged hole in the valence band and a negatively charged electron in the conduction band of a semiconductor. Hence these elementary excitations of a semiconductor are often regarded as the hydrogen analog of the solid state. It is now more than 80 years since Frenkel [1–3], Peierls [4], and Wannier [5] formulated the concept of excitons. After the experimental discovery of these quasiparticles in cuprous oxide (Cu_2O) by Gross and Karryjew in 1952 [6], excitons in bulk semiconductors became an important topic in solid-state physics from the late 1950s to the 1970s (see, e.g., Refs. [7–12] and further references therein).

Very recently, new attention has been drawn to the field of excitons by an experimental observation of the yellow exciton series in Cu_2O up to a large principal quantum number of $n = 25$ [13]. This discovery has opened up the research field of giant Rydberg excitons and led to a variety of new experimental and theoretical investigations [13–36]. Furthermore, it may pave the way, e.g., to a deeper understanding of interparticle interactions in the solid [13] and to applications in quantum information technology [27].

Even though the spectrum of Rydberg excitons in Cu_2O can be described quite well in a first approximation by the hydrogenlike model of Wannier, one must keep in mind that excitons are complex many-body states of the solid and, hence, that there are significant limitations to the hydrogenlike model and to the atomlike description of these quasiparticles [37].

Some essential corrections to the hydrogenlike model comprise, e.g., the inclusion of the complete cubic valence-band structure [38–43], which leads to a complicated fine-structure splitting, the central-cell corrections, which account for deviations from the hydrogenlike model in the limit of a small exciton radius [7,44–50], and the exchange interaction [7,47,48,51,52]. Furthermore, interactions with other quasiparticles, like, e.g., phonons have to be considered [53–55]. All of these effects have already been discussed recently for the excitons in Cu_2O [15,18,20,21,25,28].

Above all, there is another fundamental difference between atoms and excitons as regards their interaction with light. By analogy with the interaction of atoms with light, one may suppose that absorption of light in a crystal can be described as the excitation of an exciton with the simultaneous disappearance of a photon [7]. Indeed, in the weak-coupling limit, the incident light acts only as a perturbation on the different energy states or excitations of the solid like, e.g., excitons [47]. However, since the excited states in the solid are connected with a polarization and since an oscillating polarization emits again an electromagnetic wave acting back onto the incident wave, there is an interplay between light and matter. If the frequency of light is within the range of the resonance frequency of an excitation, the coupling is strong and thus anomalous dispersion can be observed [7]. Due to this coupling, excitons and photons cannot be treated as independent entities or good eigenstates, but new quasiparticles must be introduced, which are called polaritons and which represent the quanta of the mixed state of polarization and electromagnetic wave [56–63].

In this regard the $1S$ orthoexciton of Cu_2O, in particular, is of interest as for this state characteristic polariton effects like propagation beats and the conservation of coherence

over macroscopic distances have already been demonstrated experimentally [64]. Furthermore, the threefold degeneracy of this state is lifted for finite momentum of the center of mass $\hbar K$, and its oscillator strengths [65] as well as its dispersion are anisotropic [20,66–68]. All of these effects and the number of experimental results for, e.g., the oscillator strength, the $\boldsymbol{K}$-dependent spectra, and the group velocity [65], with which theoretical results can be compared, make the $1S$ orthoexciton an ideal candidate for theoretical investigations.

In this paper we present the theory of exciton-polaritons in Cu_2O. We extend the Hamiltonian of Ref. [28], which accounts for the complete valence-band structure, the exchange interaction, and the central-cell corrections, for a finite momentum $\hbar K$ of the center of mass. The corresponding Schrödinger equation can then be solved using a complete basis. This method allows us not only to calculate dipole and quadrupole oscillator strengths but also the size of the nonanalytic exchange interaction. As the splitting due to the nonanalytic exchange interaction at $K = 0$ is identical to the longitudinal-transverse splitting (LT splitting) when treating polaritons, this interaction needs to be considered for a correct treatment of the complete problem. We show how to calculate the polariton dispersion for the complete exciton spectrum.

Due to the presence of the complete valence-band structure, the exchange interaction, and the central-cell corrections, we obtain very complex polariton dispersions for the excitons in Cu_2O, which by far exceed previous investigations on the polariton dispersion using a simple hydrogenlike model [26]. The main emphasis in this paper is on the only exciton state for which a pronounced polariton effect has been observed in several experiments: the $1S$ orthoexciton state. At first, we discuss the effects of a finite momentum $\hbar\boldsymbol{K}$ of the center of mass on the spectrum. The K-dependent splitting, which has been discussed in Refs. [20,66–68], is now treated using the K-dependent Hamiltonian in explicit form and including the central-cell corrections. The calculated splittings are in the same order of magnitude as the splittings observed experimentally [66–68].

Previous publications on the $1S$ orthoexciton polariton [26,64,65,69] were confining the polariton problem to situations where the K vector is parallel to one of the principal symmetry axes of the crystal. This ensures that the polarization of the exciton is always parallel to the electric field vector and perpendicular to the wave vector. What is still missing is a proper treatment of the general polariton problem with an *arbitrary* orientation of the K vector, which considers the K-dependent splitting and the polariton effect simultaneously. The challenge is the anisotropy of the exciton-photon interaction, leading to a polarization that is neither parallel to the electric field nor orthogonal to the wave vector. Solving this very complex problem is a significant step ahead in a proper treatment of the exciton polariton problem. We are able to show that the general polariton problem can be reduced to solving an eigenvalue problem involving two photon states and three exciton states; thus giving rise to five distinct polariton branches. The general case leads to polariton states with transverse and longitudinal polarization components. These hybrid polaritons states can therefore be regarded as a mixture between a transverse polariton and a longitudinal exciton.

Using the 5×5 matrix model for the anisotropic dispersion of the $1S$ ortho-exciton-polariton, we are able to calculate the group velocity, the oscillator strengths, and spectra for different orientations of $\boldsymbol{K}$ and to compare them with experimental results [64,65,67,69]. We especially discuss the two cases of the polariton spectra in the planes perpendicular to $[1\bar{1}0]$ and [111]. In the first case, the vector $\boldsymbol{K}$ is oriented in one of the six mirror planes of the cubic group O_h so that the polariton states can be classified according to two different irreducible representations of the group C_s. As regards the second case, there is no such symmetry left and five polariton branches are obtained independently from the polarization of light. We are able to compare our results with experimental transmission spectra. The good agreement between theory and experiment not only emphasizes the special nature of the $1S$ ortho-exciton-polariton but also proves the validity of the 5×5 matrix model as a useful theoretical model for further investigations on this polariton.

Our investigations with respect to the exciton-polariton problem in Cu_2O are gaining additional importance by recent second harmonic generation (SHG) measurements performed by J. Mund *et al.* [70]. The experiments were carried out with a laser generating ultra short pulses having a band width covering several meV. The resonant excitation of the $1S$ orthoexciton by means of a two-photon absorption process generates exciton polaritons that are giving rise to SHG radiation. The polariton nature of the quadrupole exciton explains why it is possible to generate SHG in a crystal with inversion symmetry.

The paper is organized as follows. In Sec. II, we present the Hamiltonian of excitons in Cu_2O when considering a finite momentum $\hbar K$ of the center of mass and show how to solve the corresponding Schrödinger equation in a complete basis. In Sec. III, we present formulas to calculate dipole and quadrupole oscillator strengths. Having introduced the multipolariton concept of exciton-polartions in Sec. IV A, we discuss the rotating wave approximation, the nonanalytic exchange interaction and criteria for the observability of polariton effects in Secs. IV B–IV D, respectively. In Sec. V, we then use the Hamiltonian, which accounts for the complete valence-band structure, the exchange interaction, and the central-cell corrections to calculate the complex dispersion of the polaritons connected with the exciton states of $2 \leqslant n \leqslant 4$. We also discuss the observability of polariton effects. The K dependent splitting and the dispersion of the $1S$ ortho-exciton-polariton are treated separately from the other polaritons in Sec. VI. After the discussion of the splitting in Sec. VI A, we introduce the 5×5 matrix model in Sec. VI B. The dispersion of the ortho-exciton-polariton, the group velocity and the oscillator strengths are compared with experimental results in Sec. VI C. We finally give a summary and outlook in Sec. VII.

II. HAMILTONIAN

In this section, we shortly present the theory of excitons with a finite momentum of the center of mass in Cu_2O, where the cubic valence-band structure, the exchange interaction and the central-cell corrections need to be considered. The

Hamiltonian of the exciton is given by

$$H = E_g + V(\boldsymbol{r}_e - \boldsymbol{r}_h) + H_e(\boldsymbol{p}_e) + H_h(\boldsymbol{p}_h) + H_{CCC}(\boldsymbol{r}_e - \boldsymbol{r}_h) + H_{exch}(\boldsymbol{r}_e - \boldsymbol{r}_h) \quad (1)$$

with the energy E_g of the band gap. The screened Coulomb interaction V, the central cell corrections H_{CCC}, the analytic exchange exchange interaction H_{exch}, and the kinetic energies $H_e(\boldsymbol{p}_e)$ and $H_h(\boldsymbol{p}_h)$ of the electron and the hole are given in Ref. [28].

We now introduce relative and center-of-mass coordinates:

$$\boldsymbol{r} = \boldsymbol{r}_e - \boldsymbol{r}_h, \quad (2a)$$

$$\boldsymbol{R} = \boldsymbol{\alpha}\boldsymbol{r}_e + \boldsymbol{\gamma}\boldsymbol{r}_h. \quad (2b)$$

The factors $\boldsymbol{\alpha}$ and $\boldsymbol{\gamma}$ are in general 3×3 matrices with $|\det(\boldsymbol{\alpha} + \boldsymbol{\gamma})| = 1$ [42]. As the Hamiltonian (1) depends only on the relative coordinate $\boldsymbol{r} = \boldsymbol{r}_e - \boldsymbol{r}_h$ of electron and hole, the momentum of the center of mass

$$\boldsymbol{P} = \boldsymbol{p}_e + \boldsymbol{p}_h = -i\hbar(\boldsymbol{\alpha} + \boldsymbol{\gamma})\nabla_{\boldsymbol{R}} \quad (3)$$

with

$$\nabla_{\boldsymbol{r}_e} = \boldsymbol{\alpha}\nabla_{\boldsymbol{R}} + \nabla_{\boldsymbol{r}}, \quad (4a)$$

$$\nabla_{\boldsymbol{r}_h} = \boldsymbol{\gamma}\nabla_{\boldsymbol{R}} - \nabla_{\boldsymbol{r}}, \quad (4b)$$

is a constant of motion, i.e., we can set $\boldsymbol{P} = \hbar\boldsymbol{K}$ [42,71]. According to Ref. [42], the matrices $\boldsymbol{\alpha}$ and $\boldsymbol{\gamma}$ can be chosen arbitrarily, as long as $|\det(\boldsymbol{\alpha} + \boldsymbol{\gamma})| = 1$ holds, but should be adapted to the problem. Note that if we insert Eqs. (2) and (4) into the Hamiltonian (1) in general a coupling term between the relative motion and the motion of center of mass appears. Only for a specific choice of $\boldsymbol{\alpha}$ and $\boldsymbol{\gamma}$ this coupling term vanishes. However, the correct values of $\boldsymbol{\alpha}$ and $\boldsymbol{\gamma}$ are difficult to find [20,71]. In particular, the generalized relative and center of mass coordinate transformation of Ref. [20] holds only if the parameters η_i in the kinetic energy of the hole are set to zero (cf. Ref. [20]). When assuming isotropic coefficients $\boldsymbol{\alpha} = \alpha\mathbf{1}$ and $\boldsymbol{\gamma} = (1-\alpha)\mathbf{1}$ it is not possible to find a constant value of α for which the relative motion and the motion of the center of mass are decoupled. This is connected to the fact that the exciton mass in Cu_2O is not isotropic [20]. Hence the more complicated generalized transformation with 3×3 matrices would be needed.

Nevertheless, the results of the Hamiltonian are independent of the choice of $\boldsymbol{\alpha}$ and $\boldsymbol{\gamma}$. As we extend the theory of excitons in semiconductors with a cubic valence-band structure for polariton effects, we simply use the coordinates and momenta of relative and center of mass motion with $\boldsymbol{\alpha} = m_e/(m_e + m_h)\mathbf{1}$ and $\boldsymbol{\gamma} = m_h/(m_e + m_h)\mathbf{1}$ known from the hydrogen atom in the following:

$$\boldsymbol{r} = \boldsymbol{r}_e - \boldsymbol{r}_h, \quad (5a)$$

$$\boldsymbol{R} = (m_e\boldsymbol{r}_e + m_h\boldsymbol{r}_h)/(m_e + m_h), \quad (5b)$$

$$\boldsymbol{p} = (m_h\boldsymbol{p}_e - m_e\boldsymbol{p}_h)/(m_e + m_h), \quad (5c)$$

$$\boldsymbol{P} = \boldsymbol{p}_e + \boldsymbol{p}_h = \hbar\boldsymbol{K}. \quad (5d)$$

We can then write the Hamiltonian in the form

$$H = H_0 + (\hbar K)H_1 + (\hbar K)^2 H_2. \quad (6)$$

The first part H_0 is exactly the Hamiltonian of relative motion presented and discussed in Ref. [28], while the last part H_2 describes the motion of the center of mass in the degenerate band case. The term H_1 depends on the relative momentum $\boldsymbol{p}$ and thus couples the relative motion and the motion of the center of mass.

For the case that the wave vector $\boldsymbol{K}$ is oriented along one of the directions of high symmetry, i.e., along [001], [110], or [111], one can rotate the coordinate system to make the quantization axis coincide with the direction of $\boldsymbol{K}$ and then express the Hamiltonian (6) in terms of irreducible tensors [40,75–77]. Explicit expressions for H_0, H_1, and H_2 for these special orientations of the wave vector $\boldsymbol{K}$ are given in Ref. [78].

The Schrödinger equation corresponding to the Hamiltonian (6) is solved using the method presented in Refs. [20,21,28] with a complete basis. The ansatz for the exciton wave function now reads

$$|\Psi_{\nu\boldsymbol{K}}\rangle = \sum_{NLJFF_tM_{F_t}} c^{\nu\boldsymbol{K}}_{NLJFF_tM_{F_t}} |\Pi\rangle, \quad (7a)$$

$$|\Pi\rangle = |N, L; (I, S_h)\, J;\, F, S_e;\, F_t, M_{F_t}\rangle \quad (7b)$$

with complex coefficients c and the quantum numbers explained in Refs. [20,21,28]. Note that the coefficients here depend on the wave vector $\boldsymbol{K}$, which enters the Hamiltonian (6). The index ν is a number to distinguish the different exciton states.

Inserting the ansatz (7) in the Schrödinger equation $H\Psi = E\Psi$ and multiplying from the left with another basis state $\langle\Pi'|$, we obtain a matrix representation of the Schrödinger equation of the form

$$\boldsymbol{D}\boldsymbol{c} = E\boldsymbol{M}\boldsymbol{c}. \quad (8)$$

The vector $\boldsymbol{c}$ contains the coefficients of the ansatz (7). All matrix elements of H_1 and H_2, which enter the symmetric matrices $\boldsymbol{D}$ and $\boldsymbol{M}$ are given in Ref. [78]. The matrix elements of H_0 are already given in the appendices of Refs. [20] and [28]. The generalized eigenvalue problem (8) can finally be solved using an appropriate LAPACK routine [79]. All material parameters used in the calculations are listed in Table I.

III. OSCILLATOR STRENGTHS

Having solved the generalized eigenvalue problem (8), one can directly calculate the relative oscillator strengths for the transitions from the ground state of the solid to the exciton states. In this section we will derive the according formulas for dipole and quadrupole transitions. The oscillator strength is strongly connected to the interaction between the excitons and photons. According to Ref. [7] the probability per unit time for a transition from the ground state Φ_0 of the semiconductor to an exciton state $\Psi^{\sigma\tau}_{vc,\nu\boldsymbol{K}}$ is proportional to $|M|^2$ with

$$M = \int \Psi^{\sigma\tau *}_{vc,\nu\boldsymbol{K}} \left[\frac{-e}{m_0}\boldsymbol{A}_0(\boldsymbol{\kappa},\xi)\sum_{l=1}^{N} e^{i\boldsymbol{\kappa}\boldsymbol{r}_l}\boldsymbol{p}_l\right]\Phi_0 d\boldsymbol{r}_1\cdots d\boldsymbol{r}_N. \quad (9)$$

Here, $\boldsymbol{A}_0(\boldsymbol{\kappa},\xi)$ denotes the amplitude of the vector potential of the radiation field with the wave vector $\boldsymbol{\kappa}$ and the polarization ξ. N denotes the number of electrons with the coordinates $\boldsymbol{r}_l$.

TABLE I. Material parameters used in the calculations.

band gap energy	$E_g = 2.17208$ eV	[13]
electron mass	$m_e = 0.99\,m_0$	[72]
spin-orbit coupling	$\Delta = 0.131$ eV	[19]
valence-band parameters	$\gamma_1 = 1.76$	[19,20]
	$\gamma_2 = 0.7532$	[19,20]
	$\gamma_3 = -0.3668$	[19,20]
	$\eta_1 = -0.020$	[19,20]
	$\eta_2 = -0.0037$	[19,20]
	$\eta_3 = -0.0337$	[19,20]
lattice constant	$a = 0.42696$ nm	[73]
dielectric constants	$\varepsilon_{s1} = 7.5$	[74]
	$\varepsilon_{b1} = \varepsilon_{s2} = 7.11$	[74]
	$\varepsilon_{b2} = 6.46$	[74]
energy of Γ_4^--LO phonons	$\hbar\omega_{LO1} = 18.7$ meV	[48]
	$\hbar\omega_{LO2} = 87$ meV	[48]
exchange energy	$J_0 = 0.792$ eV	[28]
central-cell correction	$V_0 = 0.539$ eV	[28]

Within the scope of the simple band model the wave function of an exciton is given by

$$\Psi^{\sigma\tau}_{vc,\,\nu\boldsymbol{K}} = \sum_{\boldsymbol{q}} f_{vc\,\nu}(\boldsymbol{q})\Phi^{\sigma\tau}_{vc}(\boldsymbol{q}-\gamma\boldsymbol{K},\boldsymbol{q}+\alpha\boldsymbol{K}), \tag{10}$$

where τ and $-\sigma$ denote the spins of the electron and the hole, respectively. As we will discuss below, the spin-orbit splitting in Cu_2O does not have a perceptible effect on the oscillator strength. Hence we will keep the derivation of the formula for the oscillator strength more simple by assuming a threefold degenerate Γ_5^+ valence band and by treating the electron spin and the hole spin separately.

The envelope function $f_{vc\,\nu}(\boldsymbol{q})$ in Eq. (10) is the Fourier transform of the solution $F_{vc\,\nu}(\boldsymbol{\beta})$ of the Wannier equation [5,7],

$$f_{vc\,\nu}(\boldsymbol{q}) = \frac{1}{\sqrt{N}}\sum_{\boldsymbol{\beta}} F_{vc\,\nu}(\boldsymbol{\beta})e^{-i\boldsymbol{q}\boldsymbol{\beta}}, \tag{11}$$

with ν denoting the different exciton states. Note that the coordinate $\boldsymbol{\beta}$ is a lattice vector which in general takes only discrete values [48]. This coordinate is identical to the relative coordinate $\boldsymbol{r}$ used in Sec. II in the continuum approximation.

The wave function (10) contains a Slater determinant of Bloch functions with one electron being in a Bloch state of the conduction band and $N-1$ electrons in Bloch states of the valence bands:

$$\Phi^{\sigma\tau}_{vc}(\boldsymbol{k}_h,\boldsymbol{k}_e) = \mathcal{A}\psi_{v\boldsymbol{k}_1\alpha}\psi_{v\boldsymbol{k}_1\beta}\cdots\psi_{v\boldsymbol{k}_h\sigma}\psi_{c\boldsymbol{k}_e\tau}\cdots\psi_{v\boldsymbol{k}_N\beta}. \tag{12}$$

Here, $\mathcal{A}$ denotes the antisymmetrization operator. With the ground state of the semiconductor

$$\Phi_0 = \mathcal{A}\psi_{v\boldsymbol{k}_1\alpha}\psi_{v\boldsymbol{k}_1\beta}\cdots\psi_{v\boldsymbol{k}_i\alpha}\psi_{v\boldsymbol{k}_i\beta}\cdots\psi_{v\boldsymbol{k}_N\beta} \tag{13}$$

we can express the exciton state (10) as

$$\left|\Psi^{\sigma\tau}_{vc,\,\nu\boldsymbol{K}}\right\rangle = \sum_{\boldsymbol{q}} f_{vc\,\nu}(\boldsymbol{q})c^\dagger_{c(\boldsymbol{q}+\alpha\boldsymbol{K})\tau}c_{v(\boldsymbol{q}-\gamma\boldsymbol{K})\sigma}|\Phi_0\rangle, \tag{14}$$

using creation and annihilation operators. The operator in square brackets in Eq. (9) can be written in second quantization as

$$\sum_{nn'}\sum_{\boldsymbol{k}\boldsymbol{k}'}\sum_{\sigma'\tau'}\frac{-e}{m_0}\boldsymbol{A}_0(\boldsymbol{\kappa},\xi)\langle\psi_{n'\boldsymbol{k}'\tau'}|e^{i\boldsymbol{\kappa}\boldsymbol{r}}\,\boldsymbol{p}|\psi_{n\boldsymbol{k}\sigma'}\rangle c^\dagger_{n'\boldsymbol{k}'\tau'}c_{n\boldsymbol{k}\sigma'}. \tag{15}$$

After some transformations, using $\boldsymbol{A}_0(\boldsymbol{\kappa},\xi) = A_0(\boldsymbol{\kappa},\xi)\hat{\boldsymbol{e}}_{\xi\boldsymbol{\kappa}}$ and neglecting umklapp processes, we arrive at

$$\begin{aligned} M = {} & \frac{-e\hbar}{m_0}A_0(\boldsymbol{\kappa},\xi)N\delta_{\tau\sigma}\delta_{\boldsymbol{\kappa},\boldsymbol{K}}\sum_{\boldsymbol{q}} f^*_{vc\,\nu}(\boldsymbol{q})\int_{\mathrm{WSC}} d\boldsymbol{r} \\ & \times u^*_{c(\boldsymbol{q}+\alpha\boldsymbol{K})}(\boldsymbol{r})\hat{\boldsymbol{e}}_{\xi\boldsymbol{\kappa}}[(\boldsymbol{q}-\gamma\boldsymbol{K})u_{v(\boldsymbol{q}-\gamma\boldsymbol{K})}(\boldsymbol{r}) \\ & - i\nabla u_{v(\boldsymbol{q}-\gamma\boldsymbol{K})}(\boldsymbol{r})] \end{aligned} \tag{16}$$

with an integral over the Wigner-Seitz cell (WSC) [80].

To obtain expressions for the dipole and quadrupole oscillator strength, we use $\boldsymbol{k}\cdot\boldsymbol{p}$ perturbation theory and keep all terms up to first order in $\boldsymbol{q}$ and $\boldsymbol{K}$. It is [48,80]

$$u_{m\boldsymbol{k}}(\boldsymbol{r}) \approx u_{m\boldsymbol{0}}(\boldsymbol{r}) + \frac{\hbar}{m_0}\sum_{n\neq m}\frac{\boldsymbol{k}\cdot\boldsymbol{p}_{nm}}{(E_m-E_n)}u_{n\boldsymbol{0}}(\boldsymbol{r}) + \cdots \tag{17}$$

with $\boldsymbol{p}_{mn} = \langle u_{m\boldsymbol{0}}|\boldsymbol{p}|u_{n\boldsymbol{0}}\rangle$ and the energy $E_n = E_n(\boldsymbol{k}=\boldsymbol{0})$ of the band n at the Γ point. Due to the orthogonality of the Bloch functions, the first summand in the integral of Eq. (16) vanishes up to first order in $\boldsymbol{q}$ and $\boldsymbol{K}$. We obtain

$$\begin{aligned} M = {} & -\frac{e\hbar}{m_0^2}A_0(\boldsymbol{\kappa},\xi)\delta_{\tau\sigma}\delta_{\boldsymbol{\kappa},\boldsymbol{K}}\sum_{\boldsymbol{q}} f^*_{vc\,\nu}(\boldsymbol{q}) \\ & \times[\langle u_{c\boldsymbol{0}}|\hat{\boldsymbol{e}}_{\xi\boldsymbol{\kappa}}\cdot\boldsymbol{p}|u_{v\boldsymbol{0}}\rangle \\ & + \langle u_{c\boldsymbol{0}}|(\hat{\boldsymbol{e}}_{\xi\boldsymbol{\kappa}}\cdot\boldsymbol{p})M_v(\boldsymbol{p}\cdot(\boldsymbol{q}-\gamma\boldsymbol{K}))|u_{v\boldsymbol{0}}\rangle \\ & + \langle u_{c\boldsymbol{0}}|((\boldsymbol{q}+\alpha\boldsymbol{K})\cdot\boldsymbol{p})M_c(\boldsymbol{p}\cdot\hat{\boldsymbol{e}}_{\xi\boldsymbol{\kappa}})|u_{v\boldsymbol{0}}\rangle], \end{aligned} \tag{18}$$

where we defined

$$M_m = \sum_{n\neq m}\frac{|u_{n\boldsymbol{0}}\rangle\langle u_{n\boldsymbol{0}}|}{(E_m-E_n)}. \tag{19}$$

The sum over $\boldsymbol{q}$ can be evaluated using

$$\frac{1}{\sqrt{N}}\sum_{\boldsymbol{q}} q_i^\chi f_{vc\,\nu}(\boldsymbol{q}) = (-i)^\chi\frac{\partial^\chi}{\partial\beta_i^\chi}F_{vc\,\nu}(\boldsymbol{\beta})\bigg|_{\boldsymbol{\beta}=\boldsymbol{0}} \tag{20}$$

and we arrive at

$$\begin{aligned} M = {} & -\frac{e\hbar}{m_0^2}A_0(\boldsymbol{\kappa},\xi)\sqrt{N}\delta_{\tau\sigma}\delta_{\boldsymbol{\kappa},\boldsymbol{K}} \\ & \times\lim_{\boldsymbol{r}\to\boldsymbol{0}}[\hat{\boldsymbol{e}}_{\xi\boldsymbol{\kappa}}\cdot\boldsymbol{p}_{cv}\,F^*_{vc\,\nu}(\boldsymbol{r}) \\ & + \hat{\boldsymbol{e}}_{\xi\boldsymbol{\kappa}}\cdot(\tilde{\boldsymbol{M}}_v+\tilde{\boldsymbol{M}}_c)\cdot(i\nabla_{\boldsymbol{\beta}}F^*_{vc\,\nu}(\boldsymbol{r})) \\ & + \hat{\boldsymbol{e}}_{\xi\boldsymbol{\kappa}}\cdot(-\gamma\tilde{\boldsymbol{M}}_v+\alpha\tilde{\boldsymbol{M}}_c)\cdot(F^*_{vc\,\nu}(\boldsymbol{r})\boldsymbol{K})], \end{aligned} \tag{21}$$

where we replaced $\boldsymbol{\beta}$ with $\boldsymbol{r}$ and defined the matrices $\tilde{\boldsymbol{M}}_v$, $\tilde{\boldsymbol{M}}_c$ with the components

$$(\tilde{\boldsymbol{M}}_v)_{ij} = \langle u_{c\boldsymbol{0}}|p_iM_vp_j|u_{v\boldsymbol{0}}\rangle, \tag{22a}$$

$$(\tilde{\boldsymbol{M}}_c)_{ij} = \langle u_{c\boldsymbol{0}}|p_iM_cp_j|u_{v\boldsymbol{0}}\rangle. \tag{22b}$$

In Cu_2O it is $\boldsymbol{p}_{cv}=0$ since the valence and the conduction band have the same parity and thus the first term in Eq. (21)

vanishes. The term $\delta_{\tau\sigma}$ has to be replaced by $\sqrt{2}\delta_{S,0}$ when using the eigenstates of the total spin $S = S_\mathrm{e} + S_\mathrm{h} = \tau - \sigma$ [81].

The operators M_c and M_v are projection operators. For reasons of symmetry, these operators transform according to the irreducible representation Γ_1^+ of O_h. On the other hand, the operator $\boldsymbol{p}$ transforms according to Γ_4^-. The symmetry of the operator between the Bloch functions in Eq. (22) is, therefore,

$$\Gamma_4^- \otimes \Gamma_1^+ \otimes \Gamma_4^- = \Gamma_1^+ \oplus \Gamma_3^+ \oplus \Gamma_4^+ \oplus \Gamma_5^+. \tag{23}$$

The symmetry of the Bloch functions (without spin) is

$$\Gamma_v \otimes \Gamma_c = \Gamma_5^+ \otimes \Gamma_1^+ = \Gamma_5^+. \tag{24}$$

Hence the expression requires that the operator has the symmetry Γ_5^+ [82]. We can then consider the coupling coefficients for the case $\Gamma_4^- \otimes \Gamma_4^- \to \Gamma_5^+$. With the basis functions $|X\rangle$, $|Y\rangle$, $|Z\rangle$ of Γ_4^- and the basis functions $|\tilde{X}\rangle = |YZ\rangle$, $|\tilde{Y}\rangle = |ZX\rangle$, and $|\tilde{Z}\rangle = |XY\rangle$ of Γ_5^+, we see that, e.g., the Γ_5^+-like part of the products $|X\rangle_1|Y\rangle_2$ and $|Y\rangle_1|X\rangle_2$ transforms as $|\tilde{Z}\rangle/\sqrt{2}$. The other expressions are obtained via cyclic permutation [83].

In Sec. II, we have introduced the quasispin $I = 1$. If we compare the states $|I, M_I\rangle$ with the three functions $|u_{v\mathbf{0}}^{xy}\rangle$, $|u_{v\mathbf{0}}^{yz}\rangle$, and $|u_{v\mathbf{0}}^{zx}\rangle$ transforming according to Γ_5^+, it is [67]

$$|1,+1\rangle_I = -\left(\left|u_{v\mathbf{0}}^{yz}\right\rangle + i\left|u_{v\mathbf{0}}^{zx}\right\rangle\right)/\sqrt{2}, \tag{25a}$$

$$|1,0\rangle_I = \left|u_{v\mathbf{0}}^{xy}\right\rangle, \tag{25b}$$

$$|1,-1\rangle_I = +\left(\left|u_{v\mathbf{0}}^{yz}\right\rangle - i\left|u_{v\mathbf{0}}^{zx}\right\rangle\right)/\sqrt{2}. \tag{25c}$$

In the envelope function of the exciton, the angular dependence is given by the spherical harmonics Y_{LM}. We know that in Eq. (21) the gradient of the envelope function at $\boldsymbol{r} = \mathbf{0}$ is nonzero only if $L = 1$ holds. Furthermore, the envelope function itself vanishes at $\boldsymbol{r} = \mathbf{0}$ if $L \neq 0$ holds.

Let us assume that the light is polarized in x direction, i.e., $\hat{\boldsymbol{e}}_{\xi\boldsymbol{K}} = \hat{\boldsymbol{e}}_x$. Let us furthermore write the function $|\Psi_{\nu\boldsymbol{K}}\rangle$ of the exciton in the form of Eq. (7), where the spins, the envelope with the angular momentum L, and the function of the hole with the quasispin I enter. The dipole term in Eq. (21) is then proportional to

$$\begin{aligned}
&\lim_{\boldsymbol{r}\to\mathbf{0}} \langle S=0, M_S=0| \left(\left\langle u_{v\mathbf{0}}^{xy}\right| \frac{\partial}{\partial y} + \left\langle u_{v\mathbf{0}}^{zx}\right| \frac{\partial}{\partial z} \right) |\Psi_{\nu\boldsymbol{K}}\rangle \\
&= \lim_{r\to 0} \langle S=0, M_S=0| \frac{\partial}{\partial r} \Bigg(\langle I=1, M_I=0|(-i)\sqrt{\frac{3}{8\pi}} (\langle L=1, M_L=1| + \langle L=1, M_L=-1|) \\
&\quad - \frac{i}{\sqrt{2}} (\langle I=1, M_I=-1| + \langle I=1, M_I=1|) \sqrt{\frac{3}{4\pi}} \langle L=1, M_L=0| \Bigg) |\Psi_{\nu\boldsymbol{K}}\rangle \\
&= -i\sqrt{\frac{3}{4\pi}} \lim_{r\to 0} \frac{\partial}{\partial r} ({}_D\langle 2,1| + {}_D\langle 2,-1|) |\Psi_{\nu\boldsymbol{K}}\rangle
\end{aligned} \tag{26}$$

Here the state $|F_t, M_{F_t}\rangle_D$ for the dipole transition (D) is a short notation for

$$|(S_\mathrm{e}, S_\mathrm{h})\, S,\, I;\, I+S,\, L;\, F_t, M_{F_t}\rangle = |(1/2, 1/2)\, 0,\, 1;\, 1,\, 1;\, F_t, M_{F_t}\rangle, \tag{27}$$

in which the coupling scheme of the spins and angular momenta is different from the one of Eq. (7b) due to the requirement that S must be a good quantum number: $S_\mathrm{e} + S_\mathrm{h} = S \to (I+S) + L = F_t$. As the quantization axis, we choose the z axis, which is parallel to one of the principal axes of the crystal lattice. In an analogous way, the quadrupole term can be written as

$$\begin{aligned}
&\lim_{\boldsymbol{r}\to\mathbf{0}} \langle S=0, M_S=0| \left(\left\langle u_{v\mathbf{0}}^{xy}\right| K_y + \left\langle u_{v\mathbf{0}}^{zx}\right| K_z \right) |\Psi_{\nu\boldsymbol{K}}\rangle \\
&= \lim_{r\to 0} \langle S=0, M_S=0| \frac{1}{\sqrt{4\pi}} \langle L=0, M_L=0| \Bigg(\langle I=1, M_I=0| K_y \\
&\quad - \frac{i}{\sqrt{2}} (\langle I=1, M_I=-1| + \langle I=1, M_I=1|) K_z \Bigg) |\Psi_{\nu\boldsymbol{K}}\rangle \\
&= \lim_{r\to 0} \frac{1}{\sqrt{4\pi}} \Bigg({}_Q\langle 1,0| K_y - \frac{i}{\sqrt{2}} ({}_Q\langle 1,-1| + {}_Q\langle 1,1|) K_z \Bigg) |\Psi_{\nu\boldsymbol{K}}\rangle
\end{aligned} \tag{28}$$

with the state $|F_t, M_{F_t}\rangle_Q$ for the quadrupole transition (Q) being a short notation for

$$|(S_\mathrm{e}, S_\mathrm{h})\, S,\, I;\, I+S,\, L;\, F_t, M_{F_t}\rangle = |(1/2, 1/2)\, 0,\, 1;\, 1,\, 0;\, F_t, M_{F_t}\rangle. \tag{29}$$

Note that this state is similar to the one of Eq. (27) but only L is set to zero. We finally arrive at the following expression for the relative oscillator strength:

$$f_{\xi\nu\boldsymbol{K}}^\mathrm{rel} = \left| \lim_{r\to 0} \left[-i(\tilde{M}_v^* + \tilde{M}_c^*) \frac{\partial}{\partial r} \left\langle T_{\xi\boldsymbol{K}}^D \middle| \Psi_{\nu\boldsymbol{K}} \right\rangle + (-\gamma \tilde{M}_v^* + \alpha \tilde{M}_c^*) \frac{K}{\sqrt{6}} \left\langle T_{\xi\boldsymbol{K}}^Q \middle| \Psi_{\nu\boldsymbol{K}} \right\rangle \right] \right|^2. \tag{30}$$

For the dipole term in Eq. (30) the two states $|T^D_{\xi\boldsymbol{K}}\rangle$ are given by

$$\left|T^D_{\xi\boldsymbol{K}}\right\rangle = \sum_{i=1}^{3} \hat{e}_{\xi\boldsymbol{K}i}\left|\pi^D_i\right\rangle, \qquad \xi = 1, 2 \tag{31}$$

with the three components of the polarization vector $\hat{\boldsymbol{e}}_{\xi\boldsymbol{K}}$ and three states, which transform according to Γ_4^- [21]:

$$\left|\pi^D_x\right\rangle = \frac{i}{\sqrt{2}}[|2,\,-1\rangle_D + |2,1\rangle_D], \tag{32a}$$

$$\left|\pi^D_y\right\rangle = \frac{1}{\sqrt{2}}[|2,\,-1\rangle_D - |2,1\rangle_D], \tag{32b}$$

$$\left|\pi^D_z\right\rangle = \frac{i}{\sqrt{2}}[|2,\,-2\rangle_D - |2,2\rangle_D]. \tag{32c}$$

The state $|T^Q_{\xi\boldsymbol{K}}\rangle$ in the quadrupole term of Eq. (30) reads

$$\left|T^Q_{\xi\boldsymbol{K}}\right\rangle = \sum_{i=1}^{3} \hat{e}_{\xi\boldsymbol{K}i}\left|\pi^Q_i\right\rangle, \quad \xi = 1, 2 \tag{33}$$

with the three states which transform according to Γ_5^+ [21]:

$$\left|\pi^Q_x\right\rangle = \hat{K}_y|1,0\rangle_Q + \hat{K}_z\frac{i}{\sqrt{2}}[|1,\,-1\rangle_Q + |1,1\rangle_Q], \tag{34a}$$

$$\left|\pi^Q_y\right\rangle = \hat{K}_x|1,0\rangle_Q + \hat{K}_z\frac{1}{\sqrt{2}}[|1,\,-1\rangle_Q - |1,1\rangle_Q], \tag{34b}$$

$$\left|\pi^Q_z\right\rangle = \hat{K}_y\frac{1}{\sqrt{2}}[|1,\,-1\rangle_Q - |1,1\rangle_Q] + \hat{K}_x\frac{i}{\sqrt{2}}[|1,\,-1\rangle_Q + |1,1\rangle_Q]. \tag{34c}$$

If we now set $K = 0$ in Eq. (30), we see that we have derived the expression for the relative oscillator strength, which has already been used in Refs. [20,21].

We can finally make an assumption as regards the size of the parameters $\tilde{M}_v$ and $\tilde{M}_c$. Since in Cu_2O the uppermost valence bands as well as the lowermost conduction band have positive parity, we see from Eq. (22) that only bands with negative parity will contribute to the sums in Eq. (19). In Cu_2O, there are only two bands of negative parity, which lie 449 meV above the lowest conduction band and 5.6 eV below the highest conduction band [48]. Hence, as regards the denominators of the form $(E_m - E_n)$ in M_c and M_v, the energy difference between the Γ_7^+ and the Γ_8^+ valence band due to the spin-orbit coupling is negligible small in comparison to the energy difference between these bands and the bands of negative parity. Thus the spin-orbit coupling does not have a sizable effect on the oscillator strength. Furthermore the denominator $(E_c - E_n)$ in M_c is much smaller than the denominator $(E_v - E_n)$ in M_v and it is $M_c \gg M_v$. We therefore neglect M_v in this paper. As a consequence, to obtain absolute oscillator strengths, only one parameter η in the final expression

$$f_{\xi\nu\boldsymbol{K}} = \eta\left|\lim_{r\to 0}\left[-i\frac{\partial}{\partial r}\left\langle T^D_{\xi\boldsymbol{K}}\middle|\Psi_{\nu\boldsymbol{K}}\right\rangle + \frac{\alpha K}{\sqrt{6}}\left\langle T^Q_{\xi\boldsymbol{K}}\middle|\Psi_{\nu\boldsymbol{K}}\right\rangle\right]\right|^2 \tag{35}$$

has to be determined via a comparison with experimental values. Note the specific form of Eq. (35), where the sum of dipole and quadrupole matrix element is squared. In contrast to the hydrogenlike model, inversion symmetry is broken when considering the more precise model of Cu_2O. Hence the exciton states are mixed-parity states and, thus, an interference term occurs. Especially for the $1S$ orthoexciton, both terms in Eq. (35) are of the same magnitude. The dipole term becomes equally large as the quadrupole term for $K \neq 0$ due to a K dependent admixture of P excitons to the $1S$ orthoexciton. Even though the parameter α occurs in Eq. (35), the whole expression is independent of its value. This is related to the fact that the wave function of the exciton also depends on α.

In this paper, we choose $\boldsymbol{K}$ to be oriented in [001], [110], or [111] direction and, as in Ref. [21], we also rotate the coordinate system to make the z axis of the new coordinate system coincide with the direction of $\boldsymbol{K}$. The formulas for the oscillator strengths for the three orientations of $\boldsymbol{K}$ [84] can be derived by analogy with Ref. [21]. The consideration of these three directions of high symmetry is sufficient to determine those parameters in Sec. VI, which are needed in the 5×5 matrix model to calculate the polariton dispersion for any other direction of $\boldsymbol{K}$.

IV. EXCITON-POLARITONS

In this section, we recapitulate the quantum mechanical theory of exciton-polaritons in Sec. IV A and discuss the rotating-wave approximation in Sec. IV B. To obtain the correct treatment of the K-dependent problem, we consider the nonanalytic exchange interaction in Sec. IV C. In Sec. IV D, we shortly present the criteria for the observability of polariton effects.

A. Polariton transformation

The quantum mechanical theory of polaritons was first developed by Hopfield, Fano, and Agranovich [56–58]. According to Refs. [56,85,86], the second-quantized Hamiltonian for the interaction of excitons and photons,

$$\begin{aligned} H = \sum_{\xi\boldsymbol{K}}\Bigg[&\hbar\omega_{\xi\boldsymbol{K}}\left(a^\dagger_{\xi\boldsymbol{K}}a_{\xi\boldsymbol{K}} + \frac{1}{2}\right) \\ &+ \sum_\nu E_{\nu\boldsymbol{K}}\left(B^\dagger_{\nu\boldsymbol{K}}B_{\nu\boldsymbol{K}} + \frac{1}{2}\right) \\ &+ i\sum_\nu C_{\xi\,\nu\boldsymbol{K}}(a^\dagger_{\xi\boldsymbol{K}} + a_{\xi-\boldsymbol{K}})(B_{\nu\boldsymbol{K}} - B^\dagger_{\nu-\boldsymbol{K}}) \\ &+ \sum_\nu D_{\xi\,\nu\boldsymbol{K}}(a^\dagger_{\xi\boldsymbol{K}} + a_{\xi-\boldsymbol{K}})(a_{\xi\boldsymbol{K}} + a^\dagger_{\xi-\boldsymbol{K}})\Bigg], \end{aligned} \tag{36}$$

can be derived either from a microscopic model of excitons with the Hamiltonian describing the interaction between radiation and matter or from the equation of motion for the exciton polarization. In the Hamiltonian (36) the operators $B^\dagger_{\nu\boldsymbol{K}}$ and $B_{\nu\boldsymbol{K}}$ create and annihilate an exciton with energy $E_{\nu\boldsymbol{K}}$, respectively, and obey Bose commutation rules in the following. Likewise, the operator $a^\dagger_{\xi\boldsymbol{K}}$ ($a_{\xi\boldsymbol{K}}$) creates (annihilates) a photon with polarization ξ and energy $\hbar\omega_{\xi\boldsymbol{K}} = \hbar cK/\sqrt{\varepsilon_{b2}}$. The coupling coefficients in the exciton-photon and the

photon-photon interaction terms of Eq. (36) are given by

$$C_{\xi\,\nu\boldsymbol{K}} = \left(\frac{\kappa_{\mathrm{SI}}\pi\beta_{\xi\nu\boldsymbol{K}}E_{\nu\boldsymbol{K}}^3}{\varepsilon_{\mathrm{b2}}\hbar\omega_{\xi\boldsymbol{K}}}\right)^{\frac{1}{2}} \tag{37}$$

with $\kappa_{\mathrm{SI}} = 1/4\pi\varepsilon_0$ and

$$D_{\xi\,\nu\boldsymbol{K}} = C_{\xi\,\nu\boldsymbol{K}}^2/E_{\nu\boldsymbol{K}}. \tag{38}$$

The polarizability $\beta_{\xi\nu\boldsymbol{K}}$ is proportional to the oscillator strength of the exciton state. With our definition of the oscillator strength $f_{\xi\nu\boldsymbol{K}}$ (cf. Refs. [64,65,69]), this proportionality is given by [85,87,88]

$$\beta_{\xi\nu\boldsymbol{K}} = \varepsilon_0\varepsilon_{\mathrm{b2}}f_{\xi\nu\boldsymbol{K}}. \tag{39}$$

The Hamiltonian (36) can be diagonalized by the Hopfield transformation [56,57], which is similar to the Bogolyubov's uv transformation [89,90]: new creation and annihilation operators $p_{\mu\xi\boldsymbol{K}}^\dagger$ and $p_{\mu\xi\boldsymbol{K}}$ are introduced via

$$a_{\xi\boldsymbol{K}} = \sum_\mu [u_{\mu\xi\boldsymbol{K}}p_{\mu\xi\boldsymbol{K}} + v_{\mu\xi-\boldsymbol{K}}^* p_{\mu\xi-\boldsymbol{K}}^\dagger], \tag{40a}$$

$$B_{\nu\boldsymbol{K}} = \sum_\mu [u_{\mu\xi\nu\boldsymbol{K}}p_{\mu\xi\boldsymbol{K}} + v_{\mu\xi\nu-\boldsymbol{K}}^* p_{\mu\xi-\boldsymbol{K}}^\dagger], \tag{40b}$$

to obtain the polariton Hamiltonian

$$H = \sum_{\mu\xi\boldsymbol{K}} E_{\mu\xi\boldsymbol{K}}p_{\mu\xi\boldsymbol{K}}^\dagger p_{\mu\xi\boldsymbol{K}} + \text{const.} \tag{41}$$

with μ and $E_{\mu\xi\boldsymbol{K}}$ denoting the polariton branches and the polariton energies, respectively. The new operators must obey Bose commutation relations and the Hamiltonian shall be diagonal, i.e.,

$$[p_{\mu\xi\boldsymbol{K}}, H] = E_{\mu\xi\boldsymbol{K}}p_{\mu\xi\boldsymbol{K}} \tag{42}$$

must hold. This provides the following conditional equation for the polariton energies [58,86,91]:

$$\frac{\hbar^2c^2K^2}{E_{\mu\xi\boldsymbol{K}}^2} = \varepsilon_{\mathrm{b2}} + \sum_\nu \frac{4\pi\kappa_{\mathrm{SI}}\beta_{\xi\nu\boldsymbol{K}}}{1-(E_{\mu\xi\boldsymbol{K}}/E_{\nu\boldsymbol{K}})^2}. \tag{43}$$

Using the phase convention of Hopfield [56], the soulitons for the coefficients u and v of the polariton transformation can be obtained (see Ref. [86]). The polariton operators can also be expressed in terms of exciton and photon operators:

$$p_{\mu\xi\boldsymbol{K}} = w_{\mu\xi\boldsymbol{K}}^{(1)}a_{\xi\boldsymbol{K}} + w_{\mu\xi-\boldsymbol{K}}^{(2)*}a_{\xi-\boldsymbol{K}}^\dagger + \sum_\nu \left[z_{\mu\xi\nu\boldsymbol{K}}^{(1)}B_{\nu\boldsymbol{K}} + z_{\mu\xi\nu-\boldsymbol{K}}^{(2)*}B_{\nu-\boldsymbol{K}}^\dagger\right]. \tag{44}$$

Since all creation and annihilation operators of the three (quasi) particles obey Bose commutation relations, we can determine the coefficients w and z by evaluating

$$[p_{\mu\xi\boldsymbol{K}}, a_{\xi\boldsymbol{K}}^\dagger] = +w_{\mu\xi\boldsymbol{K}}^{(1)} = u_{\mu\xi\boldsymbol{K}}^*, \tag{45a}$$

$$[p_{\mu\xi\boldsymbol{K}}, a_{\xi-\boldsymbol{K}}] = -w_{\mu\xi\boldsymbol{K}}^{(2)*} = v_{\mu\xi\boldsymbol{K}}^*, \tag{45b}$$

and

$$[p_{\mu\xi\boldsymbol{K}}, B_{\nu-\boldsymbol{K}}^\dagger] = +z_{\mu\xi\nu\boldsymbol{K}}^{(1)} = u_{\mu\xi\nu\boldsymbol{K}}^*, \tag{46a}$$

$$[p_{\mu\xi\boldsymbol{K}}, B_{\nu\boldsymbol{K}}] = -z_{\mu\xi\nu\boldsymbol{K}}^{(2)*} = v_{\mu\xi\nu\boldsymbol{K}}^*. \tag{46b}$$

The coefficients $w_{\mu\xi\boldsymbol{K}}^{(i)}$ or the sum

$$W_{\mu\xi\boldsymbol{K}} = \sum_{i=1}^{2} |w_{\mu\xi\boldsymbol{K}}^{(i)}|^2 \tag{47}$$

then allow one to determine whether the polariton is more photonlike ($W_{\mu\xi\boldsymbol{K}} \to 1$) or more excitonlike ($W_{\mu\xi\boldsymbol{K}} \to 0$).

B. Rotating-wave approximation

In the literature, polaritons are often treated within the so-called rotating-wave approximation [85]. In this case, the term with the coefficient D and the antiresonant terms of the form aB and $a^\dagger B^\dagger$ are neglected in the Hamiltonian (36). The resulting Hamiltonian

$$H = \sum_{\xi\boldsymbol{K}}\left[\hbar\omega_{\xi\boldsymbol{K}}a_{\xi\boldsymbol{K}}^\dagger a_{\xi\boldsymbol{K}} + \sum_\nu E_{\nu\boldsymbol{K}}B_{\nu\boldsymbol{K}}^\dagger B_{\nu\boldsymbol{K}} + \sum_\nu C_{\xi\,\nu\boldsymbol{K}}(a_{\xi\boldsymbol{K}}^\dagger B_{\nu\boldsymbol{K}} + a_{\xi\boldsymbol{K}}B_{\nu\boldsymbol{K}}^\dagger)\right] \tag{48}$$

is then called the Jaynes-Cummings Hamiltonian [92], where the vacuum energy of the photons has also been neglected [85] and where the operators $a_{\xi\boldsymbol{K}}$ have been replaced with $ia_{\xi\boldsymbol{K}}$. Note that this replacement does not change the physics of the problem since it only adds global phases to the occupation-number states. The occupation-number operator and the commutation relations remain unchanged.

The coefficient $C_{\xi\,\nu\boldsymbol{K}}$ can be written as [85,88]

$$C_{\xi\,\nu\boldsymbol{K}} = \left[\frac{\kappa_{\mathrm{SI}}\pi\beta_{\xi\nu\boldsymbol{K}}E_{\nu\boldsymbol{K}}^3}{\varepsilon_{\mathrm{b2}}\hbar\omega_{\xi\boldsymbol{K}}}\right]^{\frac{1}{2}} \approx \frac{1}{2}\left(\frac{K_0}{K}\right)^{\frac{1}{2}}\hbar\Omega_{\mathrm{R}} \tag{49}$$

with the wave vector at the exciton-photon resonance $K_0 = E_{\nu \boldsymbol{K}_0}\sqrt{\varepsilon_{\mathrm{b}2}}/\hbar c$ and the Rabi frequency

$$\Omega_{\mathrm{R}} = E_{\nu \boldsymbol{K}_0}\sqrt{\frac{4\pi\kappa_{\mathrm{SI}}\beta_{\xi\nu\boldsymbol{K}}}{\varepsilon_{\mathrm{b}2}\hbar^2}}. \tag{50}$$

The rotating wave approximation is generally valid if $\hbar\Omega_{\mathrm{R}} \ll E_{\nu \boldsymbol{K}_0}$ holds. This is, e.g., the case for anorganic semiconductors and especially for Cu_2O [88].

Close to the resonance ($K \approx K_0$) one can assume $C_{\xi\,\nu\boldsymbol{K}} \approx \hbar\Omega_{\mathrm{R}}/2$. Note that for $K \to 0$ the coupling constant (49) diverges, which is *a manifestation of the infrared catastrophe in quantum electrodynamics* [85]. Hence the simplifications made above are valid only in the vicinity of the exciton-photon resonance. Otherwise, the full Hamiltonian (36) has to be diagonalized.

In the rotating-wave approximation, the polariton transformation is more simple as there is no interaction between states with different values of $\boldsymbol{K}$. Using the ansatz

$$p_{\mu\xi\boldsymbol{K}} = w_{\mu\xi\boldsymbol{K}} a_{\xi\boldsymbol{K}} + \sum_i z_{\mu\xi\nu_i\boldsymbol{K}} B_{\nu_i\boldsymbol{K}}, \tag{51}$$

the Bose commutation relations of the creation and annihilation operators, and the condition (42) for the polariton operator, one ends up with the eigenvalue problem

$$\boldsymbol{P}_{\xi\{\nu\}\boldsymbol{K}} \boldsymbol{z}_{\mu\xi\{\nu\}\boldsymbol{K}} = E_{\mu\xi\boldsymbol{K}} \boldsymbol{z}_{\mu\xi\{\nu\}\boldsymbol{K}} \tag{52}$$

with

$$\boldsymbol{P}_{\xi\{\nu\}\boldsymbol{K}} = \begin{pmatrix} \hbar\omega_{\xi\boldsymbol{K}} & \frac{1}{2}\hbar\Omega_{\mathrm{R},\,\nu_1} & \frac{1}{2}\hbar\Omega_{\mathrm{R},\,\nu_2} & \cdots & \frac{1}{2}\hbar\Omega_{\mathrm{R},\,\nu_n} & \cdots \\ \frac{1}{2}\hbar\Omega_{\mathrm{R},\,\nu_1} & E_{\nu_1\boldsymbol{K}} & 0 & \cdots & 0 & \cdots \\ \frac{1}{2}\hbar\Omega_{\mathrm{R},\,\nu_2} & 0 & E_{\nu_2\boldsymbol{K}} & & \vdots & \\ \vdots & \vdots & & \ddots & 0 & \cdots \\ \frac{1}{2}\hbar\Omega_{\mathrm{R},\,\nu_n} & 0 & \cdots & 0 & E_{\nu_n\boldsymbol{K}} & \\ \vdots & \vdots & & \vdots & & \ddots \end{pmatrix} \quad \text{and}$$

$$\boldsymbol{z}_{\mu\xi\{\nu\}\boldsymbol{K}} = \begin{pmatrix} w_{\mu\xi\boldsymbol{K}} \\ z_{\mu\xi\nu_1\boldsymbol{K}} \\ z_{\mu\xi\nu_2\boldsymbol{K}} \\ \vdots \\ z_{\mu\xi\nu_n\boldsymbol{K}} \\ \vdots \end{pmatrix}. \tag{53}$$

Knowing the energies $E_{\nu\boldsymbol{K}}$ and the Rabi frequencies $\Omega_{\mathrm{R},\,\nu}$ of the exciton states, one can directly obtain the corresponding polariton energies by determining the eigenvalues of Eq. (52).

Finally, as the polariton is a mixed state of a photon and excitons, one can again determine the photonlike part

$$W_{\mu\xi\boldsymbol{K}} = |w_{\mu\xi\boldsymbol{K}}|^2 \tag{54}$$

of the polariton or the contribution

$$Z_{\mu\xi\nu\boldsymbol{K}} = |z_{\mu\xi\nu\boldsymbol{K}}|^2 \tag{55}$$

of the exciton with the energy $E_{\nu\boldsymbol{K}}$ to the polariton.

C. Nonanalytic exchange interaction

There is another interaction affecting the exciton states: the nonanalytic (NA) exchange interaction. It is well known that the splitting caused by $H_{\mathrm{exch}}^{\mathrm{NA}}$ is identical to the longitudinal-transverse splitting (LT splitting) when treating polaritons [93]. Hence it is indispensable to include the nonanalytic exchange interaction in the theory to obtain a correct treatment of the complete problem.

In this section we will derive an expression for the nonanalytic exchange interaction. We start with the formula of Ref. [25] for the nonanalytic exchange energy between two exciton states $\Psi^{\sigma\tau}_{vc,\,\nu\boldsymbol{K}}$ and $\Psi^{\sigma'\tau'}_{vc,\,\nu'\boldsymbol{K}'}$ in second quantization:

$$H_{\mathrm{exch}}^{\mathrm{NA}} = \sum_{\nu\nu'\boldsymbol{K}} \frac{m^*_{\nu\boldsymbol{K}} m_{\nu'\boldsymbol{K}}}{\varepsilon_0\varepsilon_{\mathrm{b}2} V_{\mathrm{uc}} K^2} B^\dagger_{\nu\boldsymbol{K}} B_{\nu'\boldsymbol{K}} \tag{56}$$

with the volume V_{uc} of one unit cell and

$$m_{\nu\boldsymbol{K}} = \delta_{\sigma\tau}\frac{e}{\sqrt{N}}\sum_{\boldsymbol{q}} f_{vc\,\nu}(\boldsymbol{q})\Bigg\{-\frac{\hbar}{m_0}\frac{\boldsymbol{K}\cdot\boldsymbol{p}_{vc}}{E_v-E_c}+\frac{\hbar^2}{m_0^2}\sum_{n\neq v,c}\Bigg[\frac{[(\boldsymbol{q}-\gamma\boldsymbol{K})\cdot\boldsymbol{p}_{vn}]\,[(\boldsymbol{q}+\alpha\boldsymbol{K})\cdot\boldsymbol{p}_{nc}]}{(E_v-E_n)(E_c-E_n)} + \frac{[(\boldsymbol{q}+\alpha\boldsymbol{K})\cdot\boldsymbol{p}_{vn}]\,[(\boldsymbol{q}+\alpha\boldsymbol{K})\cdot\boldsymbol{p}_{nc}]}{(E_c-E_v)(E_c-E_n)} + \frac{[(\boldsymbol{q}-\gamma\boldsymbol{K})\cdot\boldsymbol{p}_{nc}]\,[(\boldsymbol{q}-\gamma\boldsymbol{K})\cdot\boldsymbol{p}_{vn}]}{(E_v-E_c)(E_v-E_n)}\Bigg]\Bigg\}. \tag{57}$$

Here, $m_{\nu\boldsymbol{K}}$ is a short notation for the function $m_{vc\,\nu}(\boldsymbol{K},\boldsymbol{0})$ of Ref. [25]. For the definitions of $\Psi^{\sigma\tau}_{vc,\,\nu\boldsymbol{K}}$, $f_{vc\,\nu}(\boldsymbol{q})$, and $\boldsymbol{p}_{mn}$ see Sec. III. The exchange energy includes the term $\delta_{\sigma\tau}\delta_{\sigma'\tau'}$. Introducing the total spin $S = S_{\mathrm{e}} + S_{\mathrm{h}} = \tau - \sigma$ of electron and hole, this term can be written for singlet and triplet states as $2\delta_{S,0}$ [81].

Using Eq. (20) and rearranging the different terms in Eq. (57) yields

$$m_{\nu\boldsymbol{K}} = \delta_{\sigma\tau}\frac{e\hbar^2}{m_0^2}\frac{K}{(E_c-E_v)}\lim_{\boldsymbol{r}\to\boldsymbol{0}}[(\tilde{\boldsymbol{N}}_v+\tilde{\boldsymbol{N}}_c)\cdot(-i\nabla_{\boldsymbol{r}}F_{vc\,\nu}(\boldsymbol{r}))+(-\gamma\tilde{\boldsymbol{N}}_v+\alpha\tilde{\boldsymbol{N}}_c)\cdot(F_{vc\,\nu}(\boldsymbol{r})\boldsymbol{K})] \tag{58}$$

with the matrices

$$\tilde{\boldsymbol{N}}_v = \langle u_{v\boldsymbol{0}}|\boldsymbol{p}M_v(\hat{\boldsymbol{K}}\cdot\boldsymbol{p})|u_{c\boldsymbol{0}}\rangle, \tag{59a}$$

$$\tilde{\boldsymbol{N}}_c = \langle u_{v\boldsymbol{0}}|(\hat{\boldsymbol{K}}\cdot\boldsymbol{p})M_c\boldsymbol{p}|u_{c\boldsymbol{0}}\rangle, \tag{59b}$$

and $\hat{\boldsymbol{K}} = \boldsymbol{K}/K$.

Due to the similarity between Eqs. (21) and (58), we can perform the same calculation as in Sec. III to obtain

$$m_{\nu\boldsymbol{K}} \sim K\lim_{r\to 0}\left[-i(\tilde{M}_v+\tilde{M}_c)\frac{\partial}{\partial r}\langle L^D_{\boldsymbol{K}}|\Psi_{\nu\boldsymbol{K}}\rangle+(-\gamma\tilde{M}_v+\alpha\tilde{M}_c)\frac{K}{\sqrt{6}}\langle L^Q_{\boldsymbol{K}}|\Psi_{\nu\boldsymbol{K}}\rangle\right] \tag{60}$$

with the states

$$|L^D_{\boldsymbol{K}}\rangle = \sum_{i=1}^{3}\hat{K}_i|\pi_i^D\rangle, \quad |L^Q_{\boldsymbol{K}}\rangle = \sum_{i=1}^{3}\hat{K}_i|\pi_i^Q\rangle. \tag{61}$$

As in Sec. III, we will assume $M_c \gg M_v$ so that we can finally state that $m_{\nu\boldsymbol{K}}$ is proportional to

$$K\lim_{r\to 0}\left[-i\frac{\partial}{\partial r}\langle L^D_{\boldsymbol{K}}|\Psi_{\nu\boldsymbol{K}}\rangle+\frac{\alpha K}{\sqrt{6}}\langle L^Q_{\boldsymbol{K}}|\Psi_{\nu\boldsymbol{K}}\rangle\right]. \tag{62}$$

We can see from Eq. (56) that there is no interaction between states with different values of $\boldsymbol{K}$, which is the same case as for the Hamiltonian (48) of the polariton interaction in the rotating-wave approximation. Knowing the exciton energies $E_{\nu\boldsymbol{K}}$ and the corresponding wave functions $|\Psi_{\nu\boldsymbol{K}}\rangle$, we can simultaneously diagonalize the polariton Hamiltonian and the NA-exchange Hamiltonian by solving the eigenvalue problem

$$(\boldsymbol{P}_{\xi\{\nu\}\boldsymbol{K}}+\boldsymbol{N}_{\{\nu\}\boldsymbol{K}})z_{\mu\xi\{\nu\}\boldsymbol{K}} = E_{\mu\xi\boldsymbol{K}}z_{\mu\xi\{\nu\}\boldsymbol{K}} \tag{63}$$

with the matrix

$$\boldsymbol{N}_{\{\nu\}\boldsymbol{K}} = \frac{\zeta}{\varepsilon_{\mathrm{b}2}K^2}\begin{pmatrix} 0 & 0 & 0 & \cdots & 0 & \cdots \\ 0 & m^*_{\nu_1\boldsymbol{K}}m_{\nu_1\boldsymbol{K}} & m^*_{\nu_1\boldsymbol{K}}m_{\nu_2\boldsymbol{K}} & \cdots & m^*_{\nu_1\boldsymbol{K}}m_{\nu_n\boldsymbol{K}} & \cdots \\ 0 & m^*_{\nu_2\boldsymbol{K}}m_{\nu_1\boldsymbol{K}} & m^*_{\nu_2\boldsymbol{K}}m_{\nu_2\boldsymbol{K}} & & \vdots & \\ \vdots & \vdots & & \ddots & & \cdots \\ 0 & m^*_{\nu_n\boldsymbol{K}}m_{\nu_1\boldsymbol{K}} & \cdots & & m^*_{\nu_n\boldsymbol{K}}m_{\nu_n\boldsymbol{K}} & \\ \vdots & \vdots & & \vdots & & \ddots \end{pmatrix}, \tag{64}$$

and the matrix $\boldsymbol{P}_{\xi\{\nu\}\boldsymbol{K}}$ and vector $z_{\mu\xi\{\nu\}\boldsymbol{K}}$ defined in Eq. (53). The constant parameter ζ can be determined by the fact that the splitting caused by $H^{\mathrm{NA}}_{\mathrm{exch}}$ is identical to the LT splitting.

D. Observability of polariton effects

We now shortly discuss the criteria for the observability of polariton effects, which were derived by Tait in Ref. [94]. To obtain these criteria, he included a damping term Γ in the model of polaritons since damping is always present in the solid due to the interaction between excitons and phonons or the leakage of photons out of the solid [88]:

$$\frac{\hbar^2 c^2 K^2}{E^2_{\mu\xi\boldsymbol{K}}} = \varepsilon_{\mathrm{b2}} + \sum_{\nu} \frac{4\pi\kappa_{\mathrm{SI}}\beta_{\xi\nu\boldsymbol{K}} E^2_{\nu\boldsymbol{K}}}{E^2_{\nu\boldsymbol{K}} - E^2_{\mu\xi\boldsymbol{K}} - i\Gamma E_{\mu\xi\boldsymbol{K}}}. \tag{65}$$

This equation can either be solved for a fixed wave vector K or for a fixed frequency $\omega = E_{\mu\xi\boldsymbol{K}}/\hbar$.

The first case corresponds to nonlinear optical experiments like, e.g., two-photon absorption. For this case a criterion of temporal coherence between the photon and the exciton can be derived [85,94]. As long as

$$\hbar\Gamma < \hbar\sqrt{\kappa_{\mathrm{SI}}\frac{\pi}{\varepsilon_{\mathrm{b2}}}\beta_{\xi\nu\boldsymbol{K}} E^2_{\nu\boldsymbol{K}_0}} = \frac{\hbar}{2}\Omega_{\mathrm{R}} \tag{66}$$

holds, where $\hbar\Gamma$ is the broadening of the linewidth due to damping, the polariton splitting is observable. This criterion can be interpreted in terms of Rabi oscillations, i.e., polariton effects are observable if a coherent energy transfer between an exciton and a photon is possible at least once [88]. Spatial coherence is already provided here by keeping K fixed [85].

The second case corresponds to reflectivity or absorption experiments. Here the coupling between the photon and the exciton must remain coherent during the propagation of the polariton through the solid in the presence of damping [85]. The criterion of spatial coherence reads [85,88,95]

$$\hbar\Gamma < \sqrt{\frac{16\pi}{Mc^2}\kappa_{\mathrm{SI}} E^3_{\nu\boldsymbol{K}_0}\beta_{\xi\nu\boldsymbol{K}}} = \frac{\hbar}{2}\Omega_{\mathrm{R}}\sqrt{\frac{16\varepsilon_{\mathrm{b2}}}{Mc^2}E_{\nu\boldsymbol{K}_0}}, \tag{67}$$

and it is generally more difficult to satisfy than Eq. (66) [88,96] since $\sqrt{16\varepsilon_{\mathrm{b2}}E_{\nu\boldsymbol{K}_0}/Mc^2} \ll 1$ holds for an exciton mass M on the order of m_0 and an exciton energy on the order of a few eV. The criterion (67) is equivalent to $l \gg \lambda$ with λ denoting the light wavelength and $l = v_g/\Gamma$ the mean free path of the exciton [85]. Hence polariton effects can hardly be observed in semiconductors with very shallow excitons, e.g., in GaAs [85], when using linear optical techniques. Therefore polariton effects are often investigated using nonlinear optical spectroscopic techniques due to the much less stringent criterion (66) [97,98].

V. RESULTS INCLUDING VB STRUCTURE AND CENTRAL-CELL CORRECTIONS

In this section, we will treat the exciton-polaritons with $2 \leqslant n \leqslant 4$ in Cu_2O using a Hamiltonian that accounts for the valence-band structure, the exchange interaction, the central-cell corrections, and the finite momentum $\hbar K$ of the center of mass. For the three orientations [001], [110], and [111] of $\boldsymbol{K}$ considered here, the cubic symmetry O_{h} is reduced to $C_{4\mathrm{v}}$, $C_{2\mathrm{v}}$, and $C_{3\mathrm{v}}$, respectively [82].

Excitons of even and odd parity behave differently in dependence on the momentum $\hbar K$. On the one hand, states of the odd series having the symmetry Γ_4^- and a component with $L = 1$ show a finite dipole oscillator strength at $K = 0$. Since the angular momentum L is not a good quantum number in Cu_2O and P-like exciton states are admixed to other states of odd parity at $K = 0$ [28], $P, F, H, \ldots$ states of symmetry Γ_4^- have a finite dipole oscillator strength. Hence, for these states already a splitting at $K = 0$ occurs due to the nonanalytic exchange interaction and the exciton-photon coupling, which affect the states of this symmetry.

On the other hand, the even exciton states do not have an oscillator strength at $K = 0$ and, therefore, no splitting occurs. For those even states, which have the symmetry Γ_5^+ and an $L = 0$ component at $K = 0$, the coupling to light via a finite K vector is possible. Since S-like exciton states are admixed to other states of even parity at $K = 0$ [28], $S, D, G, \ldots$ states of symmetry Γ_5^+ obtain a finite quadrupole oscillator strength being proportional to K^2.

At first, we will compare our numerical results for the relative oscillator strengths of the $1S$ excitons with the absolute value from the experiment. This will allow us to calculate absolute oscillator strengths for all exciton states. Having determined the correct size of the nonanalytic exchange interaction for the nP excitons and, hence, for all other exciton states, we can then investigate the dispersion of exciton-polaritons for the three orientations of $\boldsymbol{K}$ along the axes of high symmetry.

Since the formula derived in Sec. III allows us only to calculate relative oscillator strengths $f^{\mathrm{rel}}_{\xi\nu\boldsymbol{K}}$ but not absolute oscillator strengths for the different polarizations ξ and exciton states $\nu\boldsymbol{K}$, we determine the scaling factor η in

$$f_{\xi\nu\boldsymbol{K}} = \eta f^{\mathrm{rel}}_{\xi\nu\boldsymbol{K}} \tag{68}$$

by comparing the theoretical results for $f^{\mathrm{rel}}_{\xi\,1S\,\boldsymbol{K}}$ for the $1S$ exciton state at the exciton-photon resonance $K = K_0$ with the experimentally obtained value of [64]

$$f_{\xi\,1S\,\boldsymbol{K}} = 3.6 \times 10^{-9} \tag{69}$$

for $\boldsymbol{K} \parallel [110]$. This yields $\eta = 825.9$. Knowing this scaling factor, we can give the absolute oscillator strengths of all exciton states in the following. With this value the oscillator strengths of, e.g., the nP excitons are given by

$$f_{\xi\,nP\,\boldsymbol{K}} = 3.75 \times 10^{-4}\frac{n^2-1}{n^5}. \tag{70}$$

For a complete description of the polariton problem, we also have to include the nonanalytic exchange interaction. The splitting caused by this interaction at $\boldsymbol{K} = \boldsymbol{0}$ must exactly equal the LT splitting due to the polariton transformation. As the rotating wave approximation does not hold for $\boldsymbol{K} \to \boldsymbol{0}$, we determine at first the polariton energies $E_{\mu\xi\boldsymbol{K}}$ for the transverse exciton states via the conditional equation

$$\frac{\hbar^2 c^2 K^2}{\varepsilon_{\mathrm{b2}} E^2_{\mu\xi\boldsymbol{K}}} = 1 + \sum_{\nu}\frac{f_{\xi\nu\boldsymbol{K}}}{1 - (E_{\mu\xi\boldsymbol{K}}/E_{\nu\boldsymbol{K}})^2}, \tag{71}$$

which is obtained when using the complete exciton-photon interaction Hamiltonian [58,86,91]. The conditional equation (71) can be rewritten so that the polariton energies are the roots of the function

$$F(E_{\mu\xi\boldsymbol{K}}) = 1 - \frac{\hbar^2\omega^2_{\xi\boldsymbol{K}}}{E^2_{\mu\xi\boldsymbol{K}}} + \sum_{\nu}\frac{f_{\nu\xi\boldsymbol{K}} E^2_{\nu\boldsymbol{K}}}{E^2_{\nu\boldsymbol{K}} - E^2_{\mu\xi\boldsymbol{K}}}, \tag{72}$$

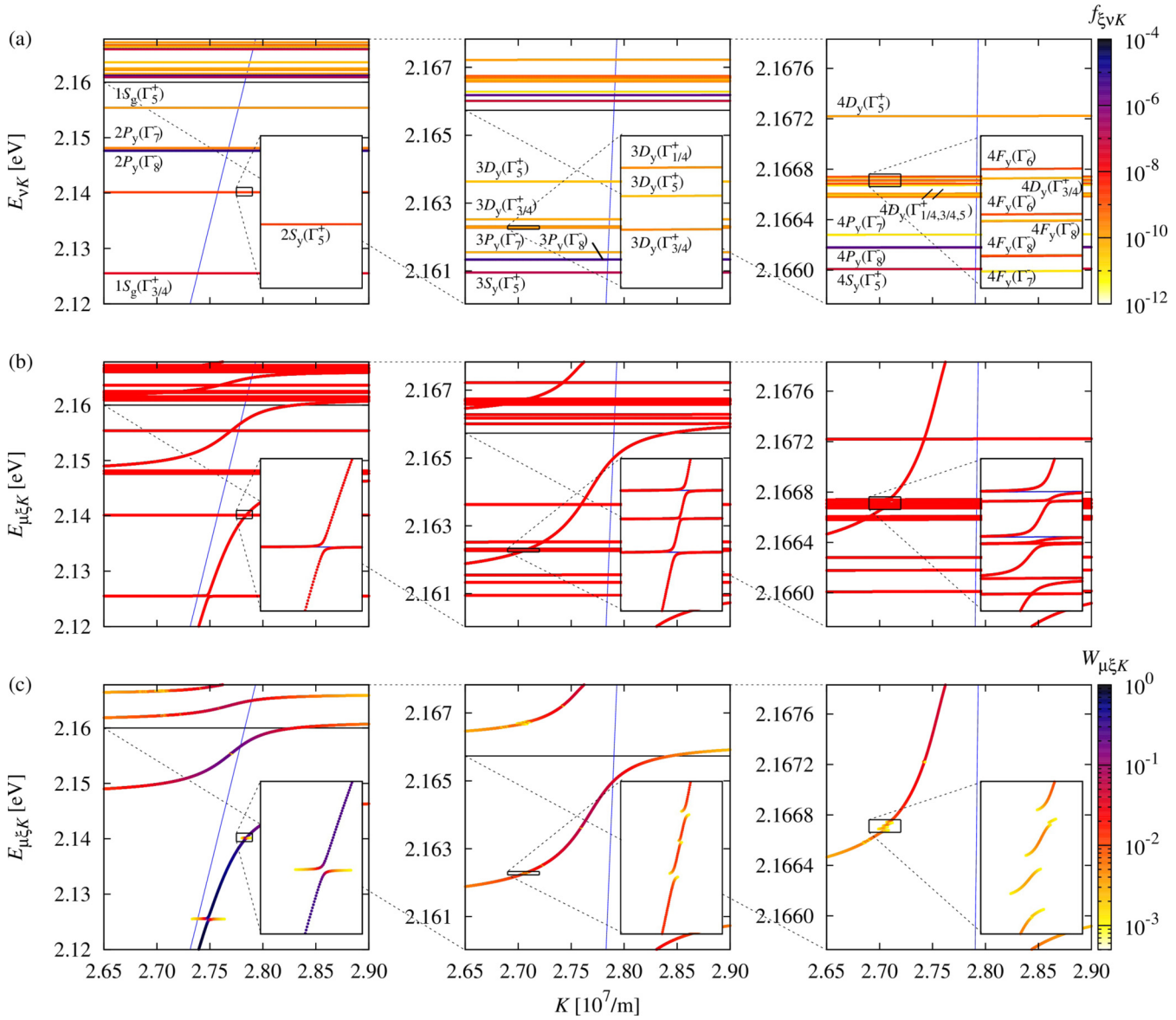

FIG. 1. (a) The exciton energies $E_{\nu\boldsymbol{K}}$ in dependence on $K = |\boldsymbol{K}|$ for $\boldsymbol{K} \parallel [001]$. Due to the inclusion of the complete valence-band structure and the central cell corrections, the spectrum is much more complicated than in the hydrogenlike case (cf. Refs. [26,99]). The color bar shows the oscillator strengths for $\xi = \sigma_z^{\pm}$ polarized light. For both polarizations the spectrum is identical. We denote from which states at $K = 0$ the exciton states originate (cf. Ref. [28]). For reasons of space, we introduce the abbreviated notation $\Gamma_{i/j}^{\pm}$ to replace $\Gamma_i^{\pm}$, $\Gamma_j^{\pm}$. The blue solid line gives the photon dispersion $\hbar\omega_{\xi\boldsymbol{K}} = \hbar K c/\sqrt{\varepsilon_{b2}}$. (b) Polariton dispersion obtained by solving the eigenvalue problem (63). Since the P excitons have a large oscillator strength, large avoided crossings can be observed. They clearly shift the position of the smaller avoided crossings for the $2S$, $3D$, and $4F$ excitons away from the position where the dispersion of light and the dispersion of these exciton states cross. (c) Photonlike part $W_{\mu\xi\boldsymbol{K}}$ of the polariton states. In all cases, the mixing of excitons and photons is strongest in the vicinity of an avoided crossing. Only for the P excitons an admixture of photons far away from the resonance occurs.

where the photon energy $\hbar\omega_{\xi\boldsymbol{K}} = \hbar K c/\sqrt{\varepsilon_{b2}}$ is used. Note that a root of $F(E_{\mu\xi\boldsymbol{K}})$ is always located between any neighboring pair of the exciton energies $E_{\nu\boldsymbol{K}}$, $E_{\nu+1\,\boldsymbol{K}}$ [100–102].

We calculate the effect of the nonanalytic exchange interaction on the longitudinal states for $\boldsymbol{K} \to \boldsymbol{0}$ by diagonalizing the matrix $\boldsymbol{N}_{\{\nu\}\boldsymbol{K}}$ given in Eq. (64). As the size of the nonanalytic exchange is *a priori* unknown, we have scaled the matrix $\boldsymbol{N}_{\{\nu\}\boldsymbol{K}}$, which describes this interaction, with a parameter ζ. We vary the parameter ζ in such a way that the energies of the longitudinal and transverse nP exciton states are identical. This yields $\zeta = 213.5 \pm 2.0$.

Of prime interest are now the polariton dispersions in the vicinity of the exciton phonon resonance. In this range of K, the rotating wave approximation is valid and we solve the eigenvalue problem (63). Note that the errors arising due to the use of the rotating-wave approximation are smaller than the error due to uncertainties in ε_{b2}.

The numerical results for $\boldsymbol{K} \parallel [001]$ are shown in Fig. 1. In the panels (a), we show the exciton spectrum in dependence on $K = |\boldsymbol{K}|$. Since the changes in the energy in dependence on K are in the order of tens of μeV, the exciton states appear as straight horizontal lines.

The spectrum is much more complicated than when using the hydrogenlike model of excitons, which was done in Refs. [26,99]. Even for vanishing momentum of the center of mass, the complete valence-band structure already leads to a complicated fine structure splitting and to a mixing of the exciton states with even or odd parity. This explains the observability of F excitons in absorption spectra due to the admixture of P excitons [18,20]. Due to the finite momentum of the center of mass S and D excitons also obtain a small oscillator strength.

We state in the panels (a) of Fig. 1 from which states at $K = 0$ the exciton states originate using the nomenclature $nL_{y/g}(\Gamma_i^{\pm})$ of Ref. [28] with the abbreviations y and g for yellow and green. In the case of the P and F excitons, we do not give the symmetry of the complete exciton state but only the combined symmetry of envelope and hole [18].

In the panels (b), we show the polariton dispersion. Only for the P excitons, which have a comparatively large oscillator strength, significant deviations between the polariton spectrum and the exciton spectrum can be observed. The insets in the panels show that also for the other exciton states avoided crossings appear due to their finite oscillator strength. However, the panels (c), which show the photonlike part of the polariton states, indicate that the mixing between excitons and photons is small in these cases.

Due to the proximity of the nS and nP states as well as that of the nF states, avoided crossings are not well separated. Hence the multipolariton concept has to be used and a single-polariton concept would lead to different results. The large avoided crossings of the P excitons clearly affect the other avoided crossings as they shift them away from the position where the dispersion of light and the dispersion of the other exciton states cross.

As regards the other orientations $\boldsymbol{K} \parallel [110]$ or $\boldsymbol{K} \parallel [111]$ of the momentum of center of mass, the differences in the polariton spectra are slight. Since the K-dependent shift of the exciton energies is on the order of tens of μeV, the exciton energies are almost the same for the three orientations of $\boldsymbol{K}$ considered. The main difference between the spectra for $\boldsymbol{K} \parallel [001]$, $\boldsymbol{K} \parallel [110]$, or $\boldsymbol{K} \parallel [111]$ is the values of the oscillator strengths due to the different symmetry breaking. Therefore also the polariton dispersions are different, however, mainly in the vicinity of the avoided crossings [103].

Note that we do not show the polariton dispersion for exciton states with $n \geqslant 5$ since the number of states with a finite oscillator strength increases rapidly. However, the oscillator strengths of the G, H, ... exciton states are very small so that polariton effects are likewise very small. Hence we do not expect to observe considerably new effects for the exciton-polaritons with $n \geqslant 5$.

Using the criteria of Tait [94] for temporal and spatial coherence presented in Sec. IV D, we can estimate the possible observability of the polariton effects. If we set $n = 2$, the criterion of temporal coherence reads

$$\hbar\Gamma < \frac{\hbar}{2}\Omega_{\mathrm{R}} \approx 6.4 \text{ meV}. \tag{73}$$

For the criterion of spatial coherence, we obtain

$$\hbar\Gamma < \frac{\hbar}{2}\Omega_{\mathrm{R}}\sqrt{\frac{16\varepsilon_{\mathrm{b2}}}{Mc^2}E_{\nu\boldsymbol{K}_0}} \approx 0.11 \text{ meV} \tag{74}$$

with the isotropic mass $M \approx 1.57m_0$ of the exciton and m_0 denoting the free electron mass. In Ref. [13], the spectrum of the giant Rydberg excitons has been investigated in an absorption experiment and, thus, experimental values of the exciton linewidths $\hbar\Gamma$ for the criterion of spatial coherence are known. For $n = 2$, the experimental line width is $\hbar\Gamma = 1.58$ meV [13,15], which is significantly larger than 0.11 meV. Therefore we expect that the polariton effects for the yellow exciton states with $n \geqslant 2$ in Cu_2O may only be observed using nonlinear spectroscopy methods and high quality crystals [97,98]. As regards the $1S$ orthoexciton state, the linewidth is small enough to clearly observe polariton effects [64,65,69].

VI. YELLOW 1S ORTHO-EXCITON-POLARITON

We now come to the yellow $1S$ ortho-exciton-polariton, for which a pronounced polariton effect has been proven in experiments. In Sec. VI A, we will discuss at first the effect of finite momentum of the center of mass $\hbar K \neq 0$ on the exciton spectrum. We will especially pay attention to the small quadrupole oscillator strength [64] and the $\boldsymbol{K}$ dependent splitting of this state [20,66–68]. In Sec. VI B, we set up a 5×5 matrix model, which allows us to calculate the anisotropic dispersion of the $1S$ ortho-exciton polariton for any direction of $\boldsymbol{K}$. We then present in Sec. VI C the polariton dispersion, determine the group velocity [65,69] as well as the spectra for rotations about the $[1\bar{1}0]$ and the [111] axis, and compare them with experimental values [65–68].

A. K-dependent splitting

As has already been stated in Sec. V, we have to consider the reduction of the irreducible representations of the cubic group O_{h} by the groups $C_{4\mathrm{v}}$, $C_{2\mathrm{v}}$, and $C_{3\mathrm{v}}$ for the three cases of $\boldsymbol{K}$ being oriented along the [001], [110], or the [111] direction, respectively. In particular, for an exciton state having the symmetry $\Gamma_5^{\pm}$ at $K = 0$, degeneracies are lifted for $K \neq 0$.

We therefore observe a splitting of the $1S_{\mathrm{y}}(\Gamma_5^+)$ orthoexciton state depending on K when solving the full K-dependent Hamiltonian of excitons in Cu_2O. This splitting is shown in Fig. 2. It was observed experimentally in Refs. [66–68] and originally discussed in terms of a K-dependent exchange interaction. However, a closer examination of this interaction revealed that it is far too weak in Cu_2O to describe the observed splitting [25]. Instead, it could be shown that the effects due to the cubic valence-band structure lead to a K-dependent effective mass and a K-dependent splitting of the $1S$ orthoexciton [20]. Hence the directional dispersion is the true cause of the experimentally observed splitting.

Note that in Ref. [20] the splitting was treated within a perturbation approach and it was already emphasized that the complete K-dependent Schrödinger equation including the central cell corrections would have to be solved to obtain correct results. This has now been done.

As the $1S$ orthoexciton state exciton state has the symmetry Γ_5^+ for $K = 0$, we expect for $\boldsymbol{K} \parallel [001]$ and $\boldsymbol{K} \parallel [111]$ a splitting into two degenerate and one nondegenerate state. For $\boldsymbol{K} \parallel [110]$ all degeneracies are lifted. This splitting can

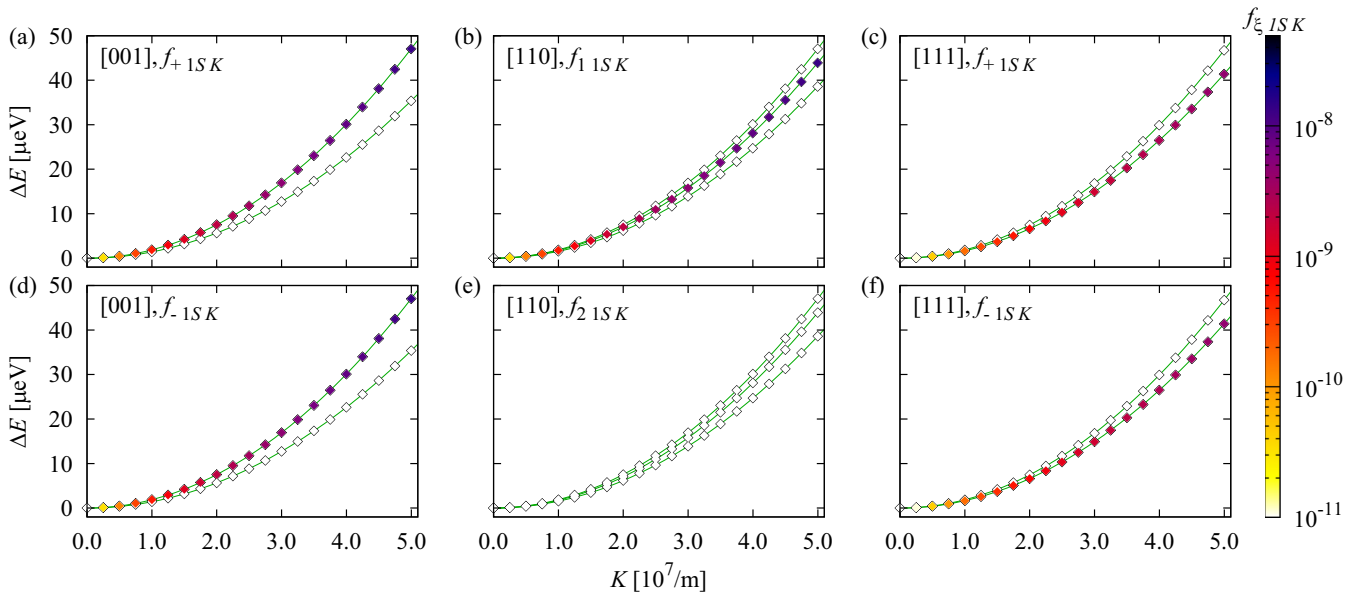

FIG. 2. Energy of the $1S_y(\Gamma_5^+)$ orthoexciton state in dependence of $K = |\boldsymbol{K}|$. We do not plot the absolute energies but the energy difference $\Delta E = E^{\mathrm{o}}_{1S,\boldsymbol{K}} - E^{\mathrm{o}}_{1S,\boldsymbol{0}}$ to show the small increase of the energy for $K \neq 0$. The $1S$ exciton obtains a finite oscillator strength for $K \neq 0$, which increases quadratically with K. Furthermore, a K-dependent splitting of the three orthoexciton states can be observed. The green solid lines are the fits of the eigenvalues of the Hamiltonian (75) to the numerical results. For further information see text.

be described by the Hamiltonian

$$\begin{aligned}\boldsymbol{H}_{\mathrm{disp}}(\boldsymbol{K}) = \Delta_1 &\begin{pmatrix} K^2 & 0 & 0 \\ 0 & K^2 & 0 \\ 0 & 0 & K^2 \end{pmatrix} \\ + \Delta_3 &\begin{pmatrix} 3K_x^2 - K^2 & 0 & 0 \\ 0 & 3K_y^2 - K^2 & 0 \\ 0 & 0 & 3K_z^2 - K^2 \end{pmatrix} \\ + \Delta_5 &\begin{pmatrix} 0 & K_xK_y & K_xK_z \\ K_xK_y & 0 & K_yK_z \\ K_xK_z & K_yK_z & 0 \end{pmatrix}. \end{aligned} \tag{75}$$

We can prove the consistency with this formula by diagonalizing the Hamiltonian (75) for $\boldsymbol{K} \parallel [001]$, $\boldsymbol{K} \parallel [110]$, and $\boldsymbol{K} \parallel [111]$ and fitting the resulting eigenvalues to our numerical results obtained with the full exciton Hamiltonian (6). This is shown in Fig. 2. The values of the fit parameters Δ_1, Δ_3, and Δ_5 are given in Table II. Since we have only three independent parameters Δ_i but seven exciton states to be fitted, the consistency is proven by the fact that we obtain the same values of the parameters Δ_i in all fits.

When performing the fit, it is not necessary to account for the K-dependent nonanalytic exchange interaction. In the next section (Sec. VI B), a formula for the size of the nonanalytic exchange interaction of the $1S$ exciton will be derived:

$$\Delta_Q = 2 f_0 E_0 / K_0^2. \tag{76}$$

Here, $f_0 = 3.6 \times 10^{-9}$ and E_0 denote the oscillator strength and the energy of the transverse exciton for $\boldsymbol{K} \parallel [001]$ at the exciton-photon resonance K_0, respectively. From the numerical results we obtain

$$K_0 = 2.614 \times 10^7 \,\frac{1}{\mathrm{m}},\; E_0 = 2.032\ \mathrm{eV}, \tag{77}$$

and, therefore,

$$\Delta_Q = 2.135 \times 10^{-17}\ \mu\mathrm{eV\,m^2}. \tag{78}$$

Obviously, the nonanalytic exchange interaction is two to three orders of magnitude smaller than the anisotropic dispersion (cf. Table II).

The experimentally observed splitting was described by the ansatz (75) as well [66–68]. When comparing the results, we have to note that the values of the Δ_i are given with respect to K_0 and that the factor Δ_1 of Refs. [66–68] only describes the "exchange interaction," i.e., the interaction without the spherically symmetric part of the kinetic energy. Therefore we have to compare $\Delta_1/K_0^2 + \hbar^2/2M$, Δ_3/K_0^2, and Δ_5/K_0^2 with our results of the parameters Δ_i. Here, $M = m_{\mathrm{e}} + m_{\mathrm{e}} \approx 1.64 m_0$ is the value of the isotropic exciton mass used in Refs. [66–68].

TABLE II. Results for the three coefficients Δ_i when fitting the eigenvalues the Hamiltonian (75) to the theoretical spectra of Fig. 2 for the different orientations of $\boldsymbol{K}$. For the [001] and the [111] directions, the values Δ_5 and Δ_3 cannot be determined, respectively. All results are given in $10^{-14}\ \mu\mathrm{eV\,m^2}$. For a comparison, we also list the experimentally determined values of Refs. [66–68]. For further information see text.

	[001]	[110]	[111]	expt
Δ_1	1.727	1.729	1.728	1.074
Δ_3	−0.156	−0.155	–	−0.189
Δ_5	–	0.213	0.213	0.292

Within our model the average mass of the $1S$ orthoexciton is

$$M = \frac{\hbar^2}{2K^2}\frac{3}{\mathrm{Tr}[\boldsymbol{H}_{\mathrm{disp}}(\boldsymbol{K})]} = \frac{\hbar^2}{2\Delta_1} = 2.2\,m_0, \tag{79}$$

which is significantly larger than the sum $M = m_\mathrm{e} + m_\mathrm{h} = m_\mathrm{e} + m_0/\gamma_1 \approx 1.56 m_0$ of the isotropic quasiparticle masses. However, there is a clear deviation from the experimentally determined value of $M = (3.0 \pm 0.2)m_0$ [104–106]. The disparity in the masses can be explained by the fact that the electron and the hole are not bare particles but polarize the surrounding lattice and are thus accompanied by clouds of longitudinal optical phonons [47]. Hence, in the experiment, always polaron masses are measured, which are larger than the bare particle masses [47]. Although we accounted for this effect via the Haken potential in the Hamiltonian, we already stated in Ref. [28] that there are some difficulties in applying this theory to Cu_2O due to the existence of two optical phonons contributing to the Fröhlich interaction and the small distance between the electron and the hole in the exciton ground state, for which the Haken potential cannot describe the non-Coulombic electron-hole interaction.

For the other two coefficients Δ_3 and Δ_5, a good agreement is obtained (see Table II), in particular, as regards the sign of the parameters. Note, however, that in Refs. [66–68], Δ_Q has been assumed to be of the same order of magnitude as the parameters Δ_i and that it has been included in the fit of the experimental data. This affects the values for Δ_3 and Δ_5 and is, therefore, another reason for the difference between the experimental and the theoretical values in Table II.

Finally, differences between the experimental and theoretical values of the parameters Δ_i could furthermore be explained by the neglect of the polariton nature of the orthoexciton in Refs. [66–68], in terms of small strains in the crystal [67] and uncertainties in the experimental values (cf. the large error bars in the figures of Ref. [66]). In particular, the fact that the experimental spectra are not identical when changing the angle of the laser beam by the same amount in opposite directions in Ref. [66] shows the presence of strains.

We wish to note that also splittings in the same order of magnitude are obtained, e.g., for the $2P$ exciton state. However, these splittings cannot be observed experimentally due to the large linewidth of the $2P$ exciton.

B. 5 × 5 matrix model

The yellow $1S$ orthoexciton is well separated from the other exciton states regarding its energy. Hence it can be treated separately from the other ones as regards polariton effects. In this section we set up a model with a 5×5 matrix, which allows calculating the dispersion of the $1S$ ortho-exciton-polariton for any direction of $\boldsymbol{K}$ close to the resonance ($K \approx K_0$). This model includes the two photon states with the polarization vectors $\hat{\boldsymbol{e}}_{\xi\boldsymbol{K}}$ and the three orthoexciton states Ψ_i, which transform according to yz, zx, and xy.

First, we will treat the oscillator strength and the Rabi frequency. Let us consider the most simple case with $\boldsymbol{K} \parallel [001]$. Due to group theoretical reasons, the three states Ψ_{yz}, Ψ_{zx}, and Ψ_{xy} are good eigenstates of the Hamiltonian. The Ψ_{zx} exciton interacts with the photon in x polarization and the Ψ_{yz} exciton interacts with the photon in y polarization. Let us denote the oscillator strength of these exciton states at the exciton-photon resonance by f_0.

For other orientations of $\boldsymbol{K}$, superpositions of the form $\sum_i a_i \Psi_i$ are eigenstates of the Hamiltonian. From the expression (35) or especially from the form of the states $|T^Q_{\xi\boldsymbol{K}}\rangle$ (33), we can see that the K-dependent oscillator strength of these exciton states is given by

$$f_{1S\,\xi\boldsymbol{K}} = f_0 \left| \begin{pmatrix} \hat{e}_{\xi\boldsymbol{K},y}K_z + \hat{e}_{\xi\boldsymbol{K},z}K_y \\ \hat{e}_{\xi\boldsymbol{K},z}K_x + \hat{e}_{\xi\boldsymbol{K},x}K_z \\ \hat{e}_{\xi\boldsymbol{K},x}K_y + \hat{e}_{\xi\boldsymbol{K},y}K_x \end{pmatrix} \cdot \begin{pmatrix} a_{yz} \\ a_{zx} \\ a_{xy} \end{pmatrix} \right|^2 \tag{80}$$

with the components $\hat{e}_{\xi\boldsymbol{K},i}$ of the polarization vector $\hat{\boldsymbol{e}}_{\xi\boldsymbol{K}}$.

For states of symmetry Γ_5^+, it has been shown in Ref. [25] that the nonanalytic exchange interaction can be written as

$$\boldsymbol{H}^{\mathrm{NA}}_{\mathrm{exch}}(\boldsymbol{K}) = \frac{\Delta_Q}{K^2} \begin{pmatrix} K_y^2K_z^2 & K_z^2K_yK_x & K_y^2K_xK_z \\ K_z^2K_yK_x & K_z^2K_x^2 & K_x^2K_yK_z \\ K_y^2K_xK_z & K_x^2K_yK_z & K_x^2K_y^2 \end{pmatrix}. \tag{81}$$

Contrary to dipole allowed excitons, the nonanalytic exchange energy depends on the fourth power of the angular coordinates of $\boldsymbol{K}$. The prefactor Δ_Q is connected to the oscillator strength and can be determined for the $1S$ state in the following way. For the special case of $\boldsymbol{K}$ being oriented in [111] direction, the Γ_5^+ state splits into one longitudinal Γ_1 and two transverse Γ_5 states. The longitudinal state is an eigenstate of the operator (81) with the eigenvalue $\Delta_Q/3$. An excitation of the longitudinal exciton leads to an oscillating longitudinal polarization. Due to the Maxwell equation $\nabla \cdot \boldsymbol{D} = 0$, the dielectric function must be zero. Hence we have

$$\varepsilon(\omega, K_0)[\Gamma_1] = \varepsilon_{\mathrm{b}2} + \frac{\frac{4}{3}f_0\varepsilon_{\mathrm{b}2}}{1 - \left(E_0 + \frac{1}{3}\Delta_Q K_0^2\right)^2/(E_0)^2} = 0 \tag{82}$$

[cf. also Eq. (71)]. Here, $E_0 = \hbar c K_0/\sqrt{\varepsilon_{\mathrm{b}2}}$ is the energy of the Γ_1 exciton at $K = K_0$ without the nonanalytic exchange interaction. Using $f_0 \ll 1$ [64,65,69], we obtain

$$\Delta_Q = 2f_0E_0/K_0^2 = 2f_0\hbar^2c^2/\varepsilon_{\mathrm{b}2}. \tag{83}$$

Combining all the K dependent effects for the $1S$ orthoexciton, we arrive at the Hamiltonian for the $1S$ ortho-exciton-polariton in the rotating-wave approximation:

$$\boldsymbol{H} = \begin{pmatrix} \boldsymbol{H}_{\mathrm{ph}} & \boldsymbol{H}_{\mathrm{exc-ph}} \\ \boldsymbol{H}^{\mathrm{T}}_{\mathrm{exc-ph}} & \boldsymbol{H}_{\mathrm{exc}} \end{pmatrix} \tag{84}$$

with the 2×2 matrix $\boldsymbol{H}_{\mathrm{ph}}$ containing the photon dispersion,

$$\boldsymbol{H}_{\mathrm{ph}} = \frac{\hbar cK}{\sqrt{\varepsilon_{\mathrm{b}2}}} \begin{pmatrix} 1 & 0 \\ 0 & 1 \end{pmatrix} = E_0\frac{K}{K_0} \begin{pmatrix} 1 & 0 \\ 0 & 1 \end{pmatrix}, \tag{85}$$

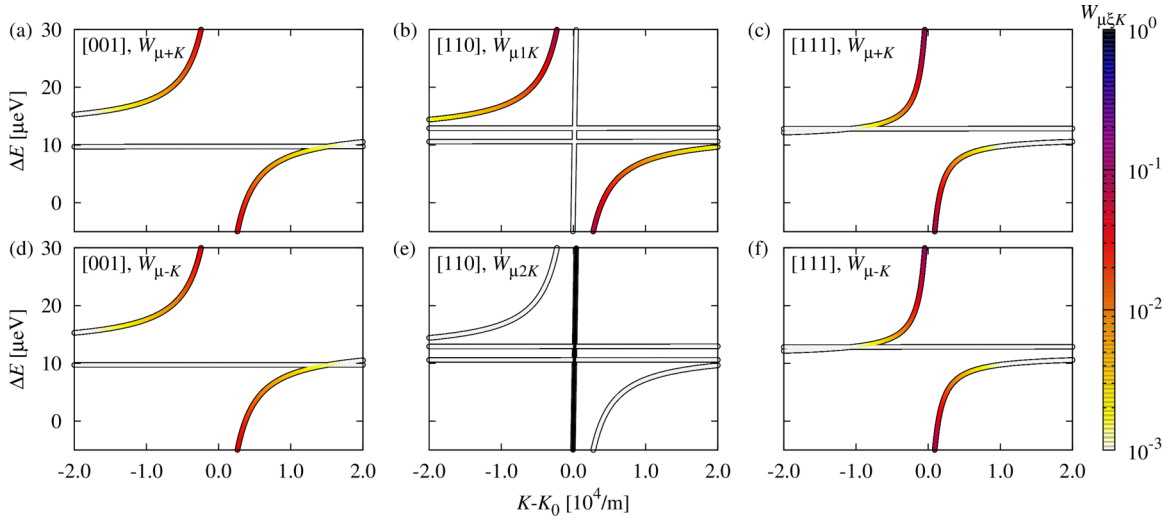

FIG. 3. Dispersion of the $1S$ ortho-exciton-polariton calculated using the 5×5 matrix model. For the different orientations of $\boldsymbol{K}$, we give the photonlike part $W_{\mu\xi\boldsymbol{K}}$ for the two polarizations ξ. It can be seen that for $\boldsymbol{K} \parallel [110]$ and light being polarized along $\hat{\boldsymbol{e}}_{2\boldsymbol{K}}$ no exciton-photon coupling occurs. We do not plot the absolute energies but the energy difference $\Delta E = E - E_0$. For further information see text.

a 2×3 matrix $\boldsymbol{H}_{\text{exc-ph}}$ with the Rabi energies $\hbar\Omega_{\text{R}} = E_0\sqrt{f_0}$,

$$\boldsymbol{H}_{\text{exc-ph}} = \frac{1}{2}\hbar\Omega_{\text{R}}\frac{1}{K_0}\begin{pmatrix} (\hat{e}_{1\boldsymbol{K},y}K_z + \hat{e}_{1\boldsymbol{K},z}K_y) & (\hat{e}_{1\boldsymbol{K},z}K_x + \hat{e}_{1\boldsymbol{K},x}K_z) & (\hat{e}_{1\boldsymbol{K},x}K_y + \hat{e}_{1\boldsymbol{K},y}K_x) \\ (\hat{e}_{2\boldsymbol{K},y}K_z + \hat{e}_{2\boldsymbol{K},z}K_y) & (\hat{e}_{2\boldsymbol{K},z}K_x + \hat{e}_{2\boldsymbol{K},x}K_z) & (\hat{e}_{2\boldsymbol{K},x}K_y + \hat{e}_{2\boldsymbol{K},y}K_x) \end{pmatrix}, \tag{86}$$

and

$$\boldsymbol{H}_{\text{exc}} = E_0\,\mathbf{1} + \boldsymbol{H}_{\text{disp}}(\boldsymbol{K}) + \boldsymbol{H}^{\text{NA}}_{\text{exch}}(\boldsymbol{K}), \tag{87}$$

where $\mathbf{1}$ is the 3×3 identity matrix.

Note that the Rabi energy depends on the square root of the oscillator strength [cf. Eq. (50)]. Hence questions about the sign of the terms $(\hat{e}_{1\boldsymbol{K},y}K_z + \hat{e}_{1\boldsymbol{K},z}K_y)$ in Eq. (86) may arise. However, for reasons of symmetry, the terms must be linear in $\boldsymbol{K}$. As the photon has negative parity, i.e., since it transforms according to Γ_4^- in O_{h}, the terms have to change the sign if the direction of $\boldsymbol{K}$ is reversed. The eigenstates of the Hamiltonian (84) can be calculated using an appropriate LAPACK routine [79].

C. Polariton dispersion

As the $1S$ orthostate shows a pronounced polariton effect, we will now come to its dispersion, which can be calculated using the 5×5 matrix model. For the subsequent calculations, we will use the parameters

$$f_0 = 3.6 \times 10^{-9}, \quad E_0 = 2.0239\ \text{eV} \tag{88}$$

of Ref. [64], which yields

$$K_0 = 2.618 \times 10^7\,\frac{1}{\text{m}}, \quad \Delta_Q = 2.135 \times 10^{-17}\ \mu\text{eV}\,\text{m}^2, \tag{89}$$

and the average values of the theoretical results for the parameters Δ_i in Table II.

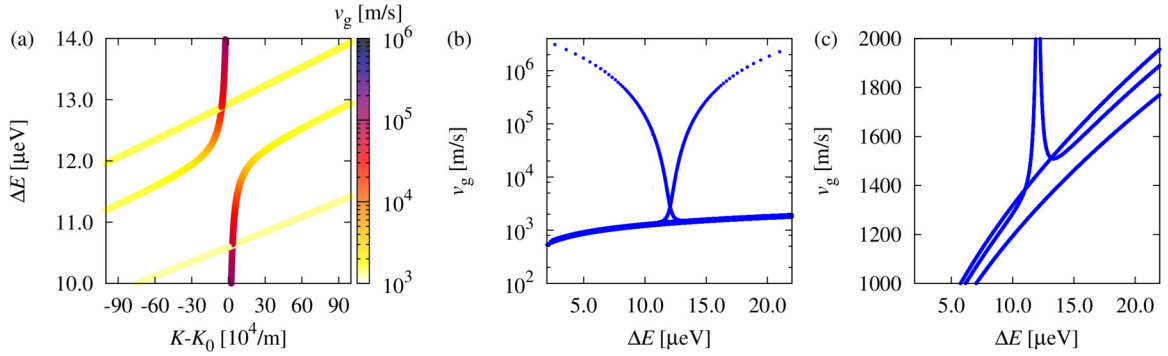

FIG. 4. (a) Group velocity v_{g} (color scale) of the $1S$ ortho-exciton-polariton with $\boldsymbol{K} \parallel [110]$ and $\hat{\boldsymbol{e}}_{1\boldsymbol{K}}$ polarization in dependence on the energy difference $\Delta E = E - E_0$ and the wave vector K. (b) and (c) The group velocity v_{g} only in dependence on the energy difference $\Delta E = E - E_0$ for a comparison with Fig. 3 of Ref. [65]. The minimum value of v_{g} depends on f_0 and is given by $v_{\text{g,min}} = 1.5$ km/s.

In Fig. 3, we first present the results for $\boldsymbol{K}$ being oriented along one of the axes of high symmetry. The longitudinal exciton states do not couple to photons and, therefore, their dispersion appears as almost horizontal lines. In particular, it can be seen that for $\boldsymbol{K} \parallel [110]$ and light being polarized along $\hat{\boldsymbol{e}}_{2\boldsymbol{K}}$ no exciton-photon coupling occurs. For the transverse states, we present the photonlike part for the two polarizations.

In Ref. [65], the group velocity of the $1S$ ortho-exciton-polariton has been measured as a function of the photon energy for $\boldsymbol{K} \parallel [110]$. From the dispersion shown in Figs. 3(b) and 3(e), we can directly calculate the group velocity via

$$v_\mathrm{g} = \frac{d\omega}{dK} = \frac{1}{\hbar}\frac{dE}{dK}. \tag{90}$$

The result is shown in Fig. 4. It can be seen that the group velocity decreases on the lower polariton branch close to the resonance for increasing values of K. However, for large values of K, the polariton dispersion approaches the exciton dispersion, which increases quadratically in K, so that v_g is then proportional to K. Hence there must be a minimum value of the group velocity. In the experiment, group velocities as low as 40 km/s could be measured [65]. However, it was not possible to measure the complete dispersion. In particular, the region of very low group velocities is not experimentally accessible. From Eq. (90) and the theoretical results, it is possible to calculate all group velocities. The minimum value of v_g obtained in our calculations is

$$v_\mathrm{g,min} = 1.5\,\frac{\mathrm{km}}{\mathrm{s}} \tag{91}$$

at $K = 2.758\ \mathrm{m}^{-1}$. When comparing our result for the group velocity, i.e., Fig. 4(b), with the experimental results of Ref. [65], a very good agreement can be observed.

From the results of the 5×5 matrix model, it is also possible to calculate the polarization vector of the photonlike part of the polariton or the orientation of the electric field as $\sum_{i=1}^{2} W_{\mu i \boldsymbol{K}} \hat{\boldsymbol{e}}_{i\boldsymbol{K}}$ and the polarization vector connected with the excitonlike part of the polariton via the symmetric cross product of $\hat{\boldsymbol{e}}_{i\boldsymbol{K}}$ and $\boldsymbol{K}$ [cf. Eq. (80)] according to the group theoretical condition $\Gamma_5^+ \otimes \Gamma_4^- \rightarrow \Gamma_4^-$. One obtains for $\Delta_3 = \Delta_5 = 0$ states with purely longitudinal or transverse polarization. However, in the general case, the states are mixed longitudinal-transverse states and the polarization is not parallel to the applied electrical field.

Another interesting point is the polariton energies if the crystal is rotated about the $[1\bar{1}0]$ or the [111] axis (cf. Refs. [66–68]). In the case that the crystal is rotated about the $[1\bar{1}0]$ plane, the K vector passes all three orientations of high symmetry from [001] to [111] and then to [110]:

$$\boldsymbol{K} = \frac{K}{\sqrt{2}}\begin{pmatrix} \sin\varphi \\ \sin\varphi \\ \sqrt{2}\cos\varphi \end{pmatrix}. \tag{92}$$

The polarization vectors are given by

$$\hat{\boldsymbol{e}}_{1\boldsymbol{K}} = \frac{1}{\sqrt{2}}\begin{pmatrix} \cos\varphi \\ \cos\varphi \\ -\sqrt{2}\sin\varphi \end{pmatrix}, \quad \hat{\boldsymbol{e}}_{2\boldsymbol{K}} = \frac{1}{\sqrt{2}}\begin{pmatrix} 1 \\ -1 \\ 0 \end{pmatrix}. \tag{93}$$

Independent of the angle φ the symmetry of the problem is always C_s [83]. This group contains the identity and a reflection

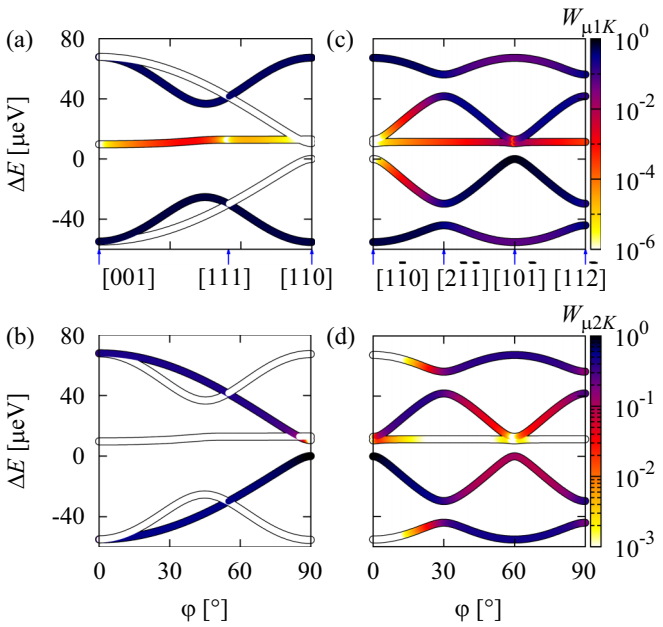

FIG. 5. (a) and (b) Polariton energies at $K = K_0$ when rotating the vector $\boldsymbol{K}$ in the plane with the normal vector $\hat{\boldsymbol{n}} = (1, -1, 0)/\sqrt{2}$. Again, we only plot the energy difference $\Delta E = E - E_0$. The color scale denotes the photonlike part of the polariton states. As is discussed in the text, the problem decouples in two problems for the two irreducible representations Γ_1 (a) and Γ_2 (b) of the group C_s. (c) and (d) Polariton energies at $K = K_0$ when rotating $\boldsymbol{K}$ in the plane with the normal vector $\hat{\boldsymbol{n}} = (1, 1, 1)/\sqrt{3}$. Every 60° $\boldsymbol{K}$ is oriented in a direction of high symmetry.

at the plane with the normal vector $\hat{\boldsymbol{n}} = (1, -1, 0)/\sqrt{2}$, which is identical to one of the six σ_d reflections of O_h. The irreducible representations of C_s are either symmetric (Γ_1) or antisymmetric (Γ_2) under reflection. Hence the complete problem falls into two parts: The linear combinations Ψ_{xy} and $(\Psi_{zx} + \Psi_{yz})/\sqrt{2}$ of the orthoexciton states transform according to Γ_1, while the linear combination $(\Psi_{zx} - \Psi_{yz})/\sqrt{2}$ transforms according to Γ_2. Furthermore, photons transform in C_s also according to Γ_1 ($\hat{\boldsymbol{e}}_{1\boldsymbol{K}}$) and Γ_2 ($\hat{\boldsymbol{e}}_{2\boldsymbol{K}}$). Therefore the problem decouples group theoretically in a Γ_1 problem with three polariton branches and a Γ_2 problem with only two polariton branches.

We keep the amount of $\boldsymbol{K}$ fixed at $K = K_0$ and increase the angle φ from 0° to 90°. The result is shown in Figs. 5(a) and 5(b). From the photonlike part of the polariton, we can clearly see the decoupling of the problem. Furthermore, the expected degeneracies of the polariton states occur if $\boldsymbol{K}$ is oriented in [001], [111], or [110] direction.

Especially, the polariton dispersion for $\boldsymbol{K} \parallel [11\bar{2}]$ ($\varphi = \arccos(-2/\sqrt{6})$) is interesting as regards second harmonic generation (SHG) measurements. This dispersion is shown in Fig. 6. SHG measurements are selective with respect to ω and K creating bulk polaritons with 2ω and $2K$. This allows the excitation of polaritons on the upper polariton branch. The lower polariton branch is inaccessible since the total K-vector is too small. Due to symmetry reasons, it is not possible to observe SHG for $\boldsymbol{K}$ being parallel to [001] or [110]. The SHG measurements in Ref. [70] were therefore

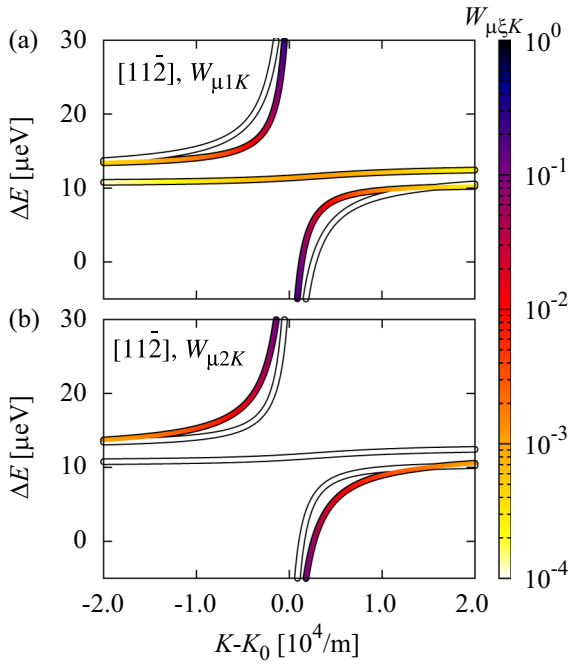

FIG. 6. Same as Fig. 3 but for $\boldsymbol{K} \parallel [11\bar{2}]$, i.e., for $\varphi = \arccos(-2/\sqrt{6})$ in Eqs. (92) and (93). In panel (a) there are three hybrid polariton branches having a polarization within the $(1,\bar{1},0)$ plane. This is in contrast to the directions of high symmetry, where only two polariton branches occur. For further information see text.

performed in a configuration where $\boldsymbol{K}$ is parallel to [111] or [11$\bar{2}$]. Especially SHG measurements with $\boldsymbol{K} \parallel [11\bar{2}]$ are interesting because there exist three hybrid polariton branches having a polarization within the $(1,\bar{1},0)$ plane. The polariton states on the upper and intermediate polariton branch are both accessible in SHG. Therefore this is a situation where two exciton polaritons can get coherently excited by means of the same nonlinear polarization $P(2\omega, 2K)$. The interference of both exciton polaritons should give rise to a polariton beat showing up in time resolved SHG measurements.

Let us now discuss the rotation about the [111] axis. The [111] axis is a threefold axis, for which reason after every 60° $\boldsymbol{K}$ is oriented in a direction of the form [110]. Between each two of these cases $\boldsymbol{K}$ is oriented in a direction of the form [112]. We have

$$\boldsymbol{K} = \frac{K}{\sqrt{6}} \begin{pmatrix} \sqrt{3}\cos\varphi + \sin\varphi \\ -\sqrt{3}\cos\varphi + \sin\varphi \\ -2\sin\varphi \end{pmatrix}, \tag{94}$$

and the polarization vectors

$$\hat{\boldsymbol{e}}_{jK} = \frac{1}{3\sqrt{j}} \begin{pmatrix} 3j - 4 + \cos\varphi - \sqrt{3}\sin\varphi \\ 3j - 4 + \cos\varphi + \sqrt{3}\sin\varphi \\ 3j - 4 - 2\cos\varphi \end{pmatrix}, \quad j = 1,2. \tag{95}$$

The resulting spectrum when varying the angle φ and keeping the amount of $\boldsymbol{K}$ fixed at $K = K_0$ is shown in Figs. 5(c) and 5(d). In the cases with $\boldsymbol{K}$ being of the form [110] only one exciton state is allowed for the polarization vector of the form [001] and all exciton states are forbidden for the other polarization vector. Note, however, that if we start with the configuration $\boldsymbol{K} \parallel [0\bar{1}0]$, $\hat{\boldsymbol{e}}_{1K} \parallel [00\bar{1}]$, and $\hat{\boldsymbol{e}}_{1K} \parallel [110]$ of Ref. [66] and perform a rotation about the [111] axis, none of the polarization vectors is oriented in the [010] direction at $\varphi = 60°$ while $\boldsymbol{K} \parallel [10\bar{1}]$ holds. Hence only for $\varphi = 0°$ all exciton states are forbidden for the polarization $\hat{\boldsymbol{e}}_{2K}$ in Figs. 5(c) and 5(d).

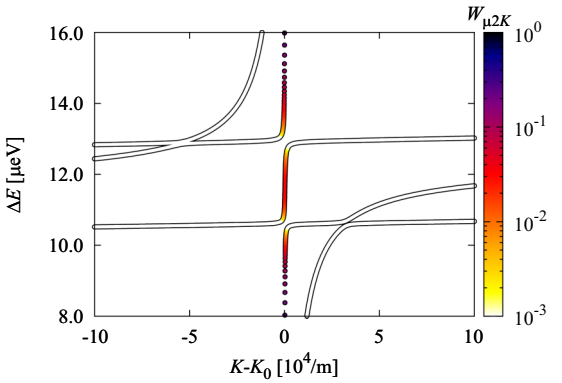

FIG. 7. Polariton energies for the vector $\boldsymbol{K}$ given by Eq. (94) with $\varphi = 4°$ and its amount is varied. Again, we only plot the energy difference $\Delta E = E - E_0$. The color scale denotes the photonlike part of the polariton states.

In the cases with $\boldsymbol{K}$ being of the form [112], all exciton states are allowed. Since the difference between $\boldsymbol{K} \parallel [1\bar{1}0]$ and $\boldsymbol{K} \parallel [2\bar{1}\bar{1}]$ are only $\Delta\varphi = 30°$, a rotation about the [111] axis with $\varphi = 4°$ already shows a significant effect on the spectrum as can be seen especially from Fig. 5(d).

Exactly for this case with $\varphi = 4°$ and the polarization $\hat{\boldsymbol{e}}_{2K}$, the transmission spectrum of the ortho-exciton-polariton is shown in Fig. 2(c) of Ref. [66]. The shape of the transmission spectrum of is clearly affected by polariton dispersion. Photons with $\boldsymbol{K} \parallel [\bar{1}10]$ and $\hat{\boldsymbol{e}}_{\xi K} \parallel [110]$ do not interact with the orthoexciton. Tilting the K vector by 4° leads to a very weak exciton photon interaction so that two of the excitons show up in this figure as two extremely narrow absorption peaks. The product of Rabi frequency and exciton lifetime is however so low that these states are excitons rather than polaritons. This explains the sharp absorption lines with a line width of less than 1 μeV. The third quadrupole-allowed state is responsible for the comparatively broad absorption line observed in [001] polarization. This state is in contrast to the other ones a perfect polariton. The much broader line width of 20 μeV is caused by polariton dispersion. If single photon spectroscopy was K-selective, this exciton polariton would show up with a similar small line width as is in the pure exciton case.

For a comparison with the experiment, we calculate the polariton dispersion for different values of K and keeping φ fixed to $\varphi = 4°$. The result is shown in Fig. 7. It can be seen that for the polarization $\hat{\boldsymbol{e}}_{2K}$ two states have a significant photon amplitude. Hence, these are the two states, which could be observed as very narrow lines in the experimental transmission spectrum [66]. However, while in the experiment the energy difference between the two states is about 4 μeV, we obtain only 2.4 μeV. We can exclude uncertainties in the parameter Δ_1 or the angle φ since a variation of these parameters does not change the size of the splitting. Only a variation of Δ_3

and Δ_5 changes the size of the splitting. However, even if we set these parameters to the experimentally determined values listed in Table II, the splitting increases only to 3.0 μeV. As we have already stated above, the presence of small strains in the crystal cannot be excluded. These may be the major reason for the observed discrepancy.

Of course, it is also possible that the positions of the transmission maxima in the experiment are not exactly given by the positions of the avoided crossings. In this case, one would have to calculate the transmission spectrum for the polariton dispersion using Pekar's boundary conditions [107]. This is likewise difficult and beyond the scope of this work. Despite all that, we obtain a good qualitative agreement with the experiment.

VII. SUMMARY AND OUTLOOK

We presented the theory of exciton-polaritons in Cu_2O. In the derivation of the formulas we accounted for all relevant effects which are needed to describe the spectra theoretically in an appropriate way, i.e., the complete valence-band structure, the exchange interaction, and the central-cell corrections [28]. This leads to a likewise complicated expression for the momentum-dependent Hamiltonian of excitons. Our method of solving the corresponding Schrödinger equation allows calculating dipole and quadrupole oscillator strengths, for which general formulas have been derived. The subsequent polariton transformation can be performed within the so-called rotating-wave approximation. Within this approximation it is straightforward to additionally account for the nonanalytic exchange interaction.

We have treated the dispersion of polaritons in Cu_2O using a multipolariton concept. When considering the correct model of excitons in Cu_2O, all states which have the symmetry Γ_5^+ for $K = 0$ obtain a finite K-dependent oscillator strength, i.e., S, D, G, and higher excitons. The more complex spectrum of excitons when using the full Hamiltonian leads to a more complex polariton dispersion than in previous works [26,99]. We also estimated that polariton effects for the yellow exciton states with $n \geqslant 2$ may only be observed using nonlinear spectroscopy methods and high quality crystals.

When including the complete valence-band structure, a K-dependent splitting of the three components of the yellow $1S$ orthoexciton appears. In contrast to Ref. [20], we have solved the complete K-dependent Schrödinger equation numerically including also the correct values for the central-cell corrections of Ref. [28]. The splittings calculated are on the same order of magnitude as the splittings observed experimentally [66–68].

As the exciton ground state is well separated from the other exciton states, it can be treated separately as regards polariton effects. Exploiting the symmetry properties of the $1S$ orthoexciton, we were able to set up a 5×5 matrix model, which allows for the calculation of the corresponding polariton dispersion for any direction of $\boldsymbol{K}$. Using the 5×5 matrix model, we investigated the dispersion of the $1S$ ortho-exciton-polariton for different orientations of $\boldsymbol{K}$. In a comparison of the results for the group velocity with experimental results, we obtained a very good agreement. The calculations allowed us to determine the minimum value of the group velocity, which is not directly accessible in the experiment, to $v_{g,\mathrm{min}} = 1.5$ km/s. We also presented results for the two special cases that the $\boldsymbol{K}$ vector is rotated in planes perpendicular to $[1\bar{1}0]$ and [111]. Especially in the second case, another comparison with experimental results was possible for a rotation angle of 4°. The splitting between the two allowed states obtained is smaller than in the experiment. This can, however, be explained in terms of the presence of small strains and uncertainties in the parameters Δ_i.

As a next step, it is possible to calculate transmission spectra from the polariton dispersion obtained via the 5×5 matrix model by assuming Pekar's boundary conditions [107] and applying the Fresnel equations. This would allow for an even better comparison of theoretical results with the experiment and may also lead to an understanding of the shape of the peaks in the spectra. Furthermore, we plan to investigate exciton spectra in an external magnetic field in Voigt configuration, where, in contrast to the Faraday configuration of Ref. [21], a finite value of the wave vector K must be considered.

ACKNOWLEDGMENTS

This work was supported by Deutsche Forschungsgemeinschaft. F.S. is grateful for support from the Landesgraduiertenförderung of the Land Baden-Württemberg. We thank M. Bayer and D. Fröhlich for fruitful discussions.

[1] J. A. Frenkel, Phys. Rev. **37**, 17 (1931).
[2] J. A. Frenkel, Phys. Rev. **37**, 1276 (1931).
[3] J. A. Frenkel, Phys. Z. Sowjetunion **9**, 533 (1936).
[4] R. Peierls, Ann. Phys. **405**, 905 (1932).
[5] G. H. Wannier, Phys. Rev. **52**, 191 (1937).
[6] E. F. Gross and I. A. Karryjew, Dokl. Akad. Nauk. SSSR **84**, 471 (1952).
[7] R. S. Knox, *Theory of Excitons*, Solid State Physics Supplement Vol. 5 (Academic, New York, 1963).
[8] V. T. Agekyan, Phys. Stat. Sol. A **43**, 11 (1977).
[9] V. M. Agranovich and V. L. Ginzburg, *Crystal Optics with spatial Dispersion and Excitons* (Springer, Berlin, 1984).
[10] G. L. Rocca, in *Electronic Excitations in Organic Based Nanostructures*, edited by V. M. Agranovich and G. F. Bassan, Thin Films and Nanostructures Vol. 31 (Elsevier, Amsterdam, 2003), pp. 97–128.
[11] A. Stahl and I. Balslev, *Electrodynamics of the Semiconductor Band Edge* (Springer, Berlin, 1987).
[12] G. Czajkowski, F. Basani, and L. Silvestri, Riv. Nuovo Cimento **26**, 1 (2003).
[13] T. Kazimierczuk, D. Fröhlich, S. Scheel, H. Stolz, and M. Bayer, Nature (London) **514**, 343 (2014).
[14] M. Aßmann, J. Thewes, D. Fröhlich, and M. Bayer, Nat. Mater. **15**, 741 (2016).

[15] F. Schweiner, J. Main, and G. Wunner, Phys. Rev. B **93**, 085203 (2016).

[16] P. Grünwald, M. Aßmann, J. Heckötter, D. Fröhlich, M. Bayer, H. Stolz, and S. Scheel, Phys. Rev. Lett. **117**, 133003 (2016).

[17] M. Feldmaier, J. Main, F. Schweiner, H. Cartarius, and G. Wunner, J. Phys. B: At. Mol. Opt. Phys. **49**, 144002 (2016).

[18] J. Thewes, J. Heckötter, T. Kazimierczuk, M. Aßmann, D. Fröhlich, M. Bayer, M. A. Semina, and M. M. Glazov, Phys. Rev. Lett. **115**, 027402 (2015), and Supplementary Material.

[19] F. Schöne, S. O. Krüger, P. Grünwald, H. Stolz, S. Scheel, M. Aßmann, J. Heckötter, J. Thewes, D. Fröhlich, and M. Bayer, Phys. Rev. B **93**, 075203 (2016).

[20] F. Schweiner, J. Main, M. Feldmaier, G. Wunner, and Ch. Uihlein, Phys. Rev. B **93**, 195203 (2016).

[21] F. Schweiner, J. Main, G. Wunner, M. Freitag, J. Heckötter, Ch. Uihlein, M. Aßmann, D. Fröhlich, and M. Bayer, Phys. Rev. B **95**, 035202 (2017).

[22] F. Schweiner, J. Main, and G. Wunner, Phys. Rev. Lett. **118**, 046401 (2017).

[23] J. Heckötter, M. Freitag, D. Fröhlich, M. Aßmann, M. Bayer, M. A. Semina, and M. M. Glazov, Phys. Rev. B **95**, 035210 (2017).

[24] S. Zielińska-Raczyńska, D. Ziemkiewicz, and G. Czajkowski, Phys. Rev. B **95**, 075204 (2017).

[25] F. Schweiner, J. Main, G. Wunner, and Ch. Uihlein, Phys. Rev. B **94**, 115201 (2016).

[26] S. Zielińska-Raczyńska, G. Czajkowski, and D. Ziemkiewicz, Phys. Rev. B **93**, 075206 (2016).

[27] S. Zielińska-Raczyńska, D. Ziemkiewicz, and G. Czajkowski, Phys. Rev. B **94**, 045205 (2016).

[28] F. Schweiner, J. Main, G. Wunner, and Ch. Uihlein, Phys. Rev. B **95**, 195201 (2017).

[29] F. Schweiner, J. Main, and G. Wunner, Phys. Rev. E **95**, 062205 (2017).

[30] F. Schweiner, P. Rommel, J. Main, and G. Wunner, Phys. Rev. B **96**, 035207 (2017).

[31] F. Schöne, H. Stolz, and N. Naka, Phys. Rev. B **96**, 115207 (2017).

[32] M. Kurz, P. Grünwald, and S. Scheel, Phys. Rev. B **95**, 245205 (2017).

[33] D. Semkat, S. Sobkowiak, F. Schöne, H. Stolz, Th. Koch, and H. Fehske, J. Phys. B: At. Mol. Opt. Phys. **50**, 204001 (2017).

[34] T. Stielow, S. Scheel, and M. Kurz, J. Phys. B: At. Mol. Opt. Phys. (to be published) [arXiv:1705.10527].

[35] J. Heckötter, M. Freitag, D. Fröhlich, M. Aßmann, M. Bayer, M. A. Semina, and M. M. Glazov, Phys. Rev. B **96**, 125142 (2017).

[36] H. Stolz, F. Schöne, and D. Semkat, arXiv:1709.00895.

[37] R. Huber, B. A. Schmid, Y. R. Shen, D. S. Chemla, and R. A. Kaindl, Phys. Rev. Lett. **96**, 017402 (2006).

[38] A. Baldereschi and N. O. Lipari, Phys. Rev. B **3**, 439 (1971).

[39] A. Baldereschi and N. O. Lipari, Phys. Rev. B **9**, 1525 (1974).

[40] A. Baldereschi and N. O. Lipari, Phys. Rev. B **8**, 2697 (1973).

[41] N. O. Lipari and M. Altarelli, Phys. Rev. B **15**, 4883 (1977).

[42] M. Altarelli and N. O. Lipari, Phys. Rev. B **15**, 4898 (1977).

[43] K. Suzuki and J. C. Hensel, Phys. Rev. B **9**, 4184 (1974).

[44] H. Haken, Il Nuovo Cimento **3**, 1230 (1956).

[45] H. Haken, in *Halbleiterprobleme IV*, edited by W. Schottky (Vieweg, Berlin, 1957), pp. 1–48.

[46] H. Haken and W. Schottky, Z. Phys. Chem. **16**, 218 (1958).

[47] C. F. Klingshirn, *Semiconductor Optics*, 3rd ed. (Springer, Berlin, 2007).

[48] G. M. Kavoulakis, Y.-C. Chang, and G. Baym, Phys. Rev. B **55**, 7593 (1997).

[49] *Polarons and Excitons*, edited by C. G. Kuper and G. D. Whitefield (Oliver and Boyd, Edinburgh, 1963).

[50] *Polarons and Excitons in Polar Semiconductors and Ionic Crystals*, edited by J. T. Devreese and F. Peeters, NATO ASI Ser. B Vol. 108 (Plenum Press, New York, 1984).

[51] K. Cho, Phys. Rev. B **14**, 4463 (1976).

[52] U. Rössler and H.-R. Trebin, Phys. Rev. B **23**, 1961 (1981).

[53] H. Fröhlich, Adv. Phys. **3**, 325 (1954).

[54] J. Bardeen and W. Shockley, Phys. Rev. **80**, 72 (1950).

[55] Y. Toyozawa, J. Phys. Chem. Solids **25**, 59 (1964).

[56] J. J. Hopfield, Phys. Rev. **112**, 1555 (1958).

[57] U. Fano, Phys. Rev. **103**, 1202 (1956).

[58] V. M. Agranovich, Zh. Eksp. Teor. Fiz. **37**, 430 (1959) [Sov. Phys. JETP **10**, 307 (1960)].

[59] J. J. Hopfield and D. G. Thomas, Phys. Rev. **132**, 563 (1963).

[60] J. B. R. Claus and L. Merten, *Light Scattering by Phonon Polaritons*, Springer Tracts Modern Physics Vol. 75 (Springer, Berlin, 1975).

[61] V. M. Agranovich and V. L. Ginzburg, *Crystal Optics with Spatial Dispersion, and Excitons*, 2nd ed., Springer Series in Solid State Sciences Vol. 42 (Springer, Berlin, 1984).

[62] B. Hönerlage, R. Lévy, J. B. Grun, C. Klingshirn, and K. Bohnert, Phys. Rep. **124**, 161 (1985).

[63] C. Klingshirn, in *Ultrafast Dynamics of Quantum Systems: Physical Processes and Spectroscopic Techniques*, edited by B. D. Bartolo, NATO ASI Ser. B Vol. 372 (Plenum Press, New York, 1998), pp. 143–211.

[64] D. Fröhlich, A. Kulik, B. Uebbing, A. Mysyrowicz, V. Langer, H. Stolz, and W. von der Osten, Phys. Rev. Lett. **67**, 2343 (1991).

[65] D. Fröhlich, G. Dasbach, G. Baldassarri, H. von Högersthal, M. Bayer, R. Klieber, D. Suter, and H. Stolz, Solid State Commun. **134**, 139 (2005).

[66] G. Dasbach, D. Fröhlich, H. Stolz, R. Klieber, D. Suter, and M. Bayer, Phys. Rev. Lett. **91**, 107401 (2003).

[67] G. Dasbach, D. Fröhlich, R. Klieber, D. Suter, M. Bayer, and H. Stolz, Phys. Rev. B **70**, 045206 (2004).

[68] G. Dasbach, D. Fröhlich, H. Stolz, R. Klieber, D. Suter, and M. Bayer, Phys. Stat. Sol C **2**, 886 (2005).

[69] D. Fröhlich, J. Brandt, C. Sandfort, M. Bayer, and H. Stolz, Phys. Stat. Sol. B **243**, 2367 (2006).

[70] J. Mund, D. Yakovlev, D. Fröhlich, and M. Bayer (unpublished).

[71] M. A. Kanehisa, Physica B+C **117-118**, 275 (1983).

[72] J. W. Hodby, T. E. Jenkins, C. Schwab, H. Tamura, and D. Trivich, J. Phys. C: Solid State Phys. **9**, 1429 (1976).

[73] H. E. Swanson and R. K. Fuyat, NBS Circular **539**, II:23 (1953).

[74] *Landolt-Börnstein*, edited by O. Madelung and U. Rössler, New Series, Group III Vol. 17 a to i, 22 a and b, 41 A to D (Springer, Berlin, 1982-2001).

[75] A. R. Edmonds, *Angular Momentum in Quantum Mechanics* (Princeton University Press, Princeton, 1960).

[76] Ch. Uihlein, D. Fröhlich, and R. Kenklies, Phys. Rev. B **23**, 2731 (1981).

[77] J. Broeckx, Phys. Rev. B **43**, 9643 (1991).
[78] See Supplemental Material at http://link.aps.org/supplemental/10.1103/PhysRevB.96.245202, for explicit expressions of H_0, H_1, and H_2 as well as the matrix elements of H_1 and H_2, which enter the symmetric matrices $\boldsymbol{D}$ and $\boldsymbol{M}$.
[79] E. Anderson, Z. Bai, C. Bischof, S. Blackford, J. Demmel, J. Dongarra, J. D. Croz, A. Greenbaum, S. Hammarling, A. McKenney *et al.*, *LAPACK Users' Guide*, 3rd ed. (Society for Industrial and Applied Mathematics, Philadelphia, PA, 1999).
[80] U. Rössler, *Solid State Theory*, 2nd ed. (Springer, Berlin, 2009).
[81] Y. Toyozawa, *Optical Processes in Solids* (Cambridge University Press, Cambridge, 2003).
[82] A. Abragam and B. Bleaney, *Electron Paramagnetic Resonance of Transition Ions* (Clarendon Press, Oxford, 1970).
[83] G. F. Koster, J. O. Dimmock, R. G. Wheeler, and H. Statz, *Properties of the Thirty-Two Point Groups* (M.I.T. Press, Cambridge, MA, 1963).
[84] See Supplemental Material at http://link.aps.org/supplemental/10.1103/PhysRevB.96.245202 for the detailed derivation of the formulas for the oscillator strengths for the three orientations of $\boldsymbol{K}$.
[85] L. C. Andreani, in *Strong Light-Matter Coupling: From Atoms to Solid-State Systems*, edited by A. Auffèves, D. Gerace, M. Richard, S. Portolan, M. F. Santos, L. C. Kwek, and C. Miniatura (World Scientific, Singapore, 2014), pp. 37–82.
[86] W. C. Tait and R. L. Weiher, Phys. Rev. **178**, 1404 (1969).
[87] J. Schmutzler, D. Fröhlich, and M. Bayer, Phys. Rev. B **87**, 245202 (2013).
[88] J. Schmutzler, Ph.D. thesis, Technische Universität Dortmund, 2014.
[89] N. N. Bogolyubov, Nuovo Cimento **7**, 794 (1958).
[90] N. N. Bogolyubov, J. Phys. USSR **11**, 23 (1947).
[91] C. Mavroyannis, J. Math. Phys. **8**, 1515 (1967).
[92] E. T. Jaynes and F. W. Cummings, Proc. IEEE **51**, 89 (1963).
[93] M. Born and K. Huang, *Dynamical Theory of Crystal Lattices* (Oxford University Press, London, 1954).
[94] W. C. Tait, Phys. Rev. B **5**, 648 (1972).
[95] V. A. Kiselev, B. S. Razbirin, and I. N. Uraltsev, Phys. Stat. Sol. B **72**, 161 (1975).
[96] D. D. Sell, S. E. Stokowski, R. Dingle, and J. V. DiLorenzo, Phys. Rev. B **7**, 4568 (1973).
[97] D. Fröhlich, in *Nonlinear Spectroscopy of Solids: Advances and Applications*, edited by B. Di. Bartolo and B. Bowlby, NATO ASI Series B Vol. 339 (Plenum Press, New York, 1994), pp. 289–326.
[98] D. Fröhlich, St. Kirchhoff, P. Köhler, and W. Nieswand, Phys. Rev. B **40**, 1976 (1989).
[99] J. Ertl, Bachelor thesis, Universität Stuttgart, 2017.
[100] N. J. Stor, I. Slapničar, and J. L. Barlow, Lin. Alg. Appl. **464**, 62 (2015).
[101] C. F. Borges and W. B. Gragg, in *Numerical Linear Algebra and Scientific Computing*, edited by L. Reichel, A. Ruttan, and R. S. Varga (de Gruyter, Berlin, 1993), pp. 11–29.
[102] D. P. O'Leary and G. W. Stewart, J. Comput. Phys. **90**, 497 (1990).
[103] See Supplemental Material at http://link.aps.org/supplemental/10.1103/PhysRevB.96.245202, which includes the polariton dispersions for $\boldsymbol{K} \parallel [110]$ and $\boldsymbol{K} \parallel [111]$.
[104] P. Y. Yu and Y. R. Shen, Phys. Rev. B **12**, 1377 (1975).
[105] D. W. Snoke, D. Braun, and M. Cardona, Phys. Rev. B **44**, 2991 (1991).
[106] P. Y. Yu and Y. R. Shen, Phys. Rev. Lett. **32**, 939 (1974).
[107] S. I. Pekar, Sov. Phys. JETP **6**, 785 (1958).